Lawrence Berkeley National Laboratory
Recent Work

Title
INFLUENCES OF GASEOUS ENVIRONMENT ON LOW GROWTH-RATE FATIGUE CRACK PROPAGATION IN STEELS

Permalink
https://escholarship.org/uc/item/4m45k9sq

Authors
Ritchie, R.O.
Suresh, S.
Topolsky, J.

Publication Date
1981-09-01

Lawrence Berkeley Laboratory

## UNIVERSITY OF CALIFORNIA

Materials & Molecular Research Division

NOV 4 1981

LI...
CU...ON

INFLUENCES OF GASEOUS ENVIRONMENT ON LOW GROWTH-RATE
FATIGUE CRACK PROPAGATION IN STEELS

Suresh, and J. Toplosky

LBL-13421

DISCLAIMER

Department of Mechanical Engineering
Massachusetts Institute of Technology
Cambridge, Massachusetts 02139

INFLUENCES OF GASEOUS ENVIRONMENT ON

LOW GROWTH-RATE FATIGUE CRACK

PROPAGATION IN STEELS

by

R.O. Ritchie*, S. Suresh* and J. Toplosky

NOTICE
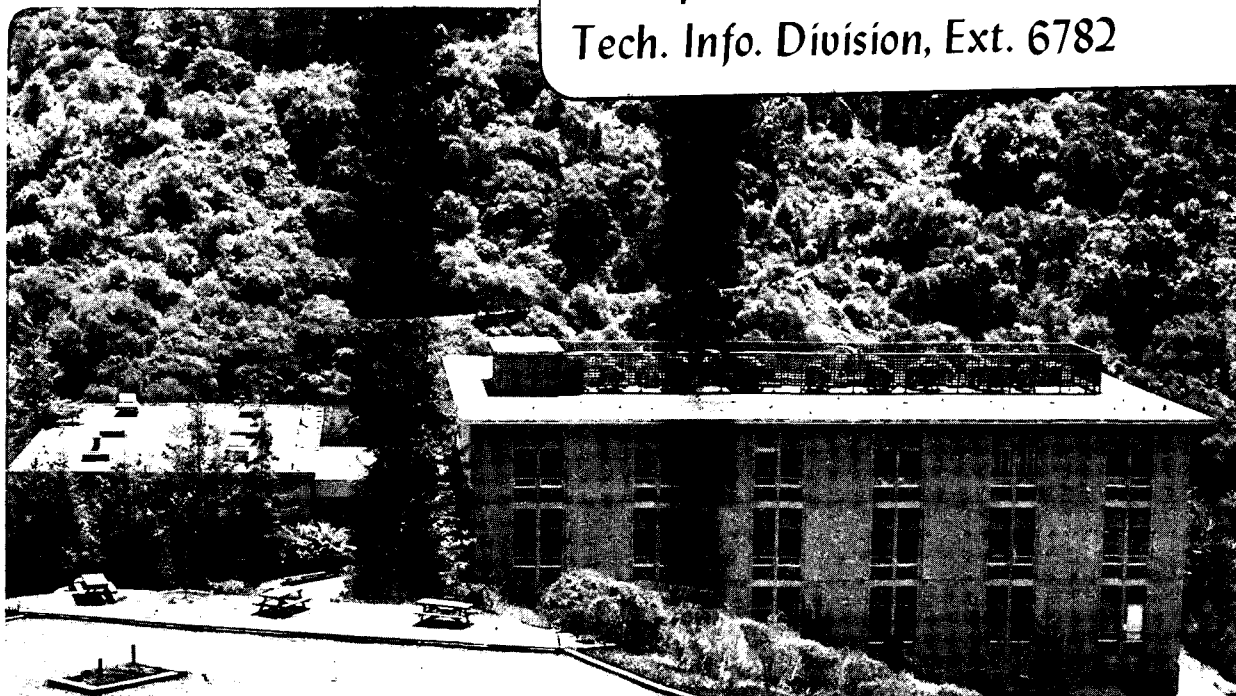
This report was prepared as an account of work sponsored by an agency of the United States Government. Neither the United States nor any agency thereof, nor any of their employees, makes any warranty, expressed or implied, or assumes any legal liability and responsibility for any third party's use or the results of such use of any information apparatus, product, or process disclosed in this report, or represents that its use by such third party would not infringe privately owned rights.

TABLE OF CONTENTS

INFLUENCES OF GASEOUS ENVIRONMENT ON LOW GROWTH RATE
FATIGUE CRACK PROPAGATION IN STEELS

R. O. Ritchie, S. Suresh and J. Toplosky
(Contract No. DE-AC02-79ER10389. A000)

FOREWARD

INFLUENCES OF GASEOUS ENVIRONMENT OF LOW GROWTH RATE
FATIGUE CRACK PROPAGATION IN STEELS

R. O. Ritchie, S. Suresh and J. Toplosky
D.O.E. Final Report No. DOE/ER/10389-2

ABSTRACT

Lower strength steels have traditionally been considered to be immune to embrittlement in the presence of hydrogen gas. In this work, it is demonstrated that contrary to conventional wisdom, there are two regions of fatigue crack growth where hydrogen gas causes significant accelerations in crack propagation rates compared to air. Environmental influences in these two regimes are shown to be dominated by entirely different mechamisms.

In particular, in the near-threshold region of fatigue crack propagation (growth rates smaller than 10^{-6} mm/cycle), it is seen that with reference to a moist air environment, near-threshold crack growth rates are accelerated in dry hydrogen gas and in dry helium, are marginally decelerated in distilled water and remain the same in wet hydrogen. Such surprising results are interpreted in terms of a new approach termed "oxide-induced crack closure" which is seen to be consistent with several hitherto unexplained experimental observations. Evidence in support of this model has been obtained indirectly using Auger spectroscopy and ESCA analyses of fracture surface oxide deposits in ferritic/bainitic, and martensitic steels. Direct evidence for oxide-induced crack closure is provided with the aid of ultrasonic techniques. Effects of variable amplitude loads, in the form of block underload cycles below threshold, are explained based on this mechanism and their implications are noted with particular reference to the measurement of fatigue thresholds.

Such results in lower strength steels are compared with corrosion fatigue crack growth behavior in ultrahigh strength steels. It is noted that although oxide-induced crack closure concepts still are valid, the effect is minimized in higher strength alloys and behavior is dominated at both near-threshold and higher growth rates by hydrogen embrittlement mechanisms.

The consequences of this work are examined in the light of the role of environment, microstructure, load ratio and strength level in influcnece ultralow growth rate fatigue crack propagation behavior in steels.

NOMENCLATURE

a	crack length
a*	crack length over which retardation occurs
c_H	local hydrogen concentration at point of maxiumum dilatation ahead of crack tip
c_o	equilibrium hydrogen concentration in unstressed lattice
d	excess oxide thickness measured on fracture surface
da/dN	fatigue crack growth rate per cycle
$(da/dN)_B$	baseline fatigue crack growth rate at ΔK_B
$(da/dN)_S$	initial fatigue crack growth rate following underload
D	diffusion coefficient for hydrogen permeation
E	elastic modulus
h_o	initial asperity height
h	final asperity height
K_I	linear elastic stress intensity factor (Mode I)
K_{Ic}	plane strain fracture toughness
K_{max}	maximum stress intensity during fatigue cycle
K_{min}	minimum stress intensity during fatigue cycle
K_{max}^T	transition maximum stress intensity
K_{Iscc}	threshold stress intensity for environmental attack
ℓ	half the distance between location of peak oxide layer and crack tip
N	number of cycles
N*	number of cycles over which retardation occurs
n'	work hardening exponent (cyclic)
R	load ratio (K_{max}/K_{min})
R_o	universal gas constant
t	time
T	absolute temperature
$\bar{v}$	partial molar volume of hydrogen in iron (2 cm^3/mole)
x	hydrogen permeation distance ahead of the crack tip
ΔCTOD	cyclic crack tip opening displacement
ΔK	alternating stress intensity range ($K_{max} - K_{min}$)
ΔK_B	baseline alternating stress intensity range

ΔK_{eff}	effective stress intensity range
ΔK_{max}^{T}	transition stress intensity range in mid-growth regime
ΔK_{o}	threshold stress intensity range for crack growth (measured)
ΔK_{th}	actual threshold stress intensity range
ΔK_{U}	alternating stress intensity range at underload
ΔK_{UC}	critical value of underload stress intensity range
$\Delta \sigma_{H}$	reduction in cohesive strength due to hydrogen
ε_{f}	true fracture strain
σ	hydrostatic tension
σ_{y}	monotonic yield strength
ν	Poisson's ratio

1. INTRODUCTION

1.1 Conceptual Background

Modern approaches to design against fatigue failure involve the application of linear elastic fracture mechanics and take into consideration that all engineering components contain incipient flaws. The useful life span of such components, then, is estimated from the number of cycles or time to propagate the largest undetected crack to a critical size which is assessed based on fracture mechanics considerations. In view of the increasing use of this "defect tolerant" approach in design, a large number of investigators have attempted to characterize the fatigue crack growth behavior of many engineering materials in terms of such variables as mean stress, frequency, microstructure, environment, and so forth. Although, a major portion of these data has been generated for the mid-growth regime of crack growth (growth rates typically in excess of 10^{-5} mm/cycle), there has been a rapidly growing need for fatigue data pertaining to extremely low growth rates (less than 10^{-6} mm/cycle or of the order of one lattice spacing per cycle) where the stress intensity range ΔK approaches a so-called threshold value ΔK_o, below which cracks remain dormant or grow at experimentally undetectable rates (1).

The use of threshold data has been found to be essential in such applications as large scale nuclear and coal conversion pressure vessels, turbine shafts, turbine blades, alternator rotors, and acoustic fatigue of welds in gas circuitry in nuclear reactor systems where high frequency, low amplitude loads may be present (1).

It is now well known from the available information that crack growth rates are sensitive to several mechanical and microstructural variables, such as mean stress or load ratio (characterized by $R = K_{min}/K_{max}$), prior stress history, grain size, grain boundary composition, crack size, cyclic frequency, monotonic and cyclic yield strength, and so forth. A recent review of the effects of these variables can be found in Ref. 1. The various mechanisms associated with the propagation of fatigue cracks are summarized schematically in Fig. 1 for the near-threshold regime as well as for higher growth rates.

The effect of environment on near-threshold fatigue behavior of
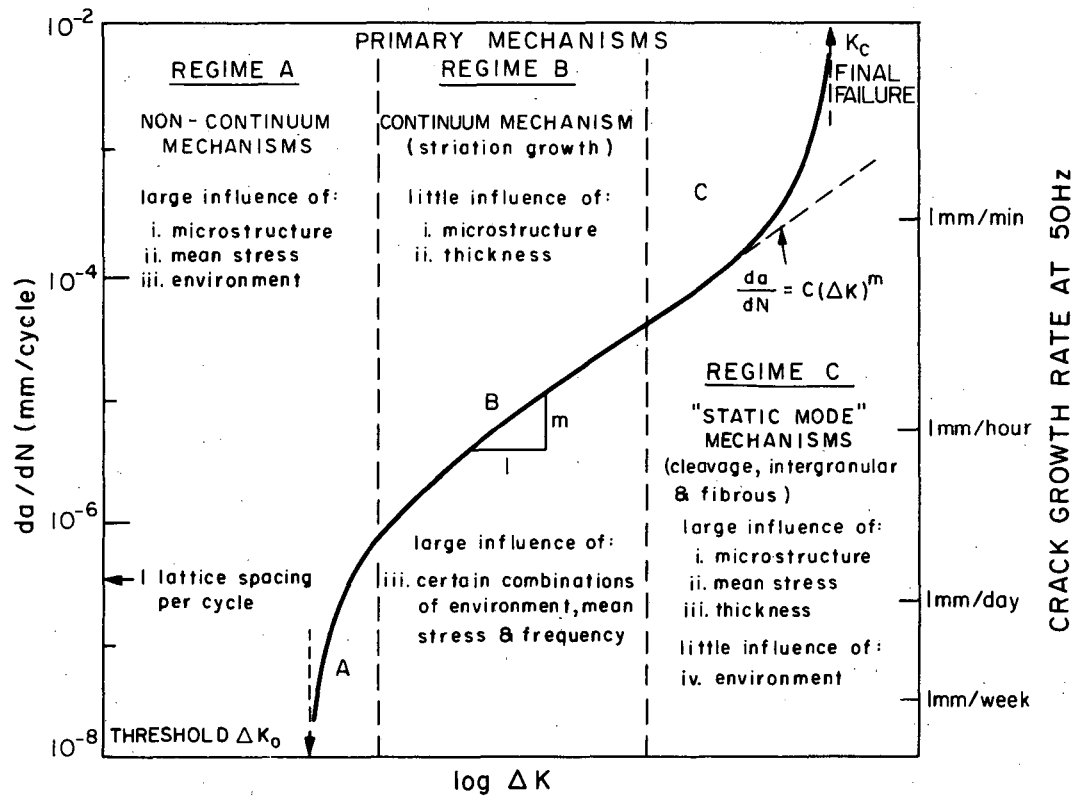
Figure 1. Schematic variation of fatigue crack growth rate with the stress intensity range in steels, showing primary crack growth mechanisms.

materials, however, has remained a subject of some controversy. Firstly, there is little information available in the literature on environmental influences at near-threshold levels. Such limited data has resulted in contradicting interpretations and inconsistent descriptions.

Fatigue tests on low carbon steel (2) and normalized pressure vessel steel (3) show significant accelerations in crack propagation rates near threshold and marked decreases in threshold ΔK_o values in presence of dehumidified hydrogen gas compared to humid air. This influence of hydrogen was explained in terms of conventional corrosion fatigue processes involving hydrogen embrittlement arguments, even though no precise mechanism for hydrogen embrittlement was suggested (4). Other results (5-7), however, were found to be inconsistent with these conventional mechanisms. For example, data on A533 B low strength nuclear pressure vessel steel (5) tested in air and distilled water show no variation in threshold behavior with change in environment for tests at a frequency of 160 Hz. Similar tests on a T-1 low strength steel (6) did not reveal any appreciable change in behavior between environments of air, distilled water, and gaseous hydrogen of unspecified purity. Results in high strength D6ac steel showed that the threshold stress intensity range values were unchanged in air and dry and wet argon atmospheres at 100-374 Hz, although near-threshold growth rates were marginally lower in dry argon compared to air (8). Furthermore, Tu and Seth (9) repored reduced near-threshold growth rates and higher ΔK_o values in the seemingly more aggressive environment of steam compared to air at 100°C.

On the other hand, several studies have found that vacuum increases the threshold ΔK_o compared to air. Threshold data on high purity heats of tempered E24 steel (10) and 13% Cr martensitic stainless steels (En 56 and FV 520b) (11) have clearly demonstrated that the near-threshold growth rates are decreased and threshold ΔK_o values are increased in vacuo compared to air. The possibility of crack flank re-welding has been suggested as a partial reason for this behavior (1). The results of Skelton and Haigh (12), however, show that in zero-tension loading it is possible to propagate cracks in vacuum to much lower values of ΔK_o than the threshold values in air.

It is evident from the above discussion that conventional corrosion fatigue mechanisms do not fully explain the wide variety of near-threshold environmental influences on steels cited in the literature. Also, arguments based on hydrogen embrittlement are inconsistent with the traditional notion that low strength steels are relatively immune to hydrogen damage at low stress values. Moreover, the purity levels of the vacuum and inert gases used in different studies are too different to allow any reasonable comparisons. Although, it has been speculated for a number of years that corrosion deposits on crack faces might play some role in determining the rates of crack growth, no quantitative analysis has yet been carried out to substantiate the exact nature of this influence.

In light of the above discussions, it is clear that with the limited extent of information available in the literature, it is not possible to make any viable mechanistic interpretations for environmental influences at threshold stress intensity levels and that no model, proposed thus far, is capable of providing possible explanations for the experimental observations.

The purpose of this program was to establish a realiable data base for environmentally-influenced near-threshold fatigue crack growth in lower strength steels and to develop mechanisms to explain the precise role of the environment in affecting crack growth behavior.

1.2 Scope of Present Study

In the present study, it is demonstrated that the significant influences of environment in the mid-growth and in the near-threshold regions of fatigue crack propagation are dominated by entirely different mechanisms (Section 3). A new approach termed "oxide-induced crack closure" is developed to explain the role of environment near threshold and is shown to be consistent with experimental observations in a low strength pressure vessel (Section 4). It is seen that at low load ratios, near-threshold growth rates are significantly reduced in moist environments (such as water or air) compared to dry environments (such as hydrogen or helium) due to the formation of excess corrosion deposits crack faces which enhances crack closure in low strength steels. The significance of oxide-induced crack closure to near-threshold corrosion

fatigue in pressure vessel steels tested in air, water, hydrogen and helium is noted. In particular, a characterization of crack flank oxide deposits is made using X-ray photoelectron spectroscopy and Auger spectroscopy. Evidence supporting the concepts of oxide-induced crack closure is provided in Section 5. The consequences of these observations are highlighted with particular reference to the measurement of near-threshold data and an explanation for the effect of underloads on fatigue crack growth at low stress intensities is given (Section 6). Mechanisms for environmentally-affected threshold behavior in lower strength pressure vessel steels are contrasted with behavior in an ultrahigh strength steel 300-M, heat treated to two different strength levels (Section 7). It is shown that in the higher strength alloys crack closure mechanisms are less important and near-threshold corrosion fatigue behavior is more governed by hydrogen embrittlement mechanisms. Additional contributions to crack closure at low stress intensities are noted in Section 8, and the relevance of these mechanisms to the role of microstructure is discussed briefly.

It is considered that the results of this program provide a clearer definition of the mechanics and mechanisms of near-threshold corrosion fatigue in steels, which can be utilized to provide a basis for the alloy design of materials with superior resistance to environmentally-influenced fracture.

2. MATERIALS AND EXPERIMENTAL PROCEDURES

2.1 Materials

The principal material used in the present investigation was a lower strength 2-1/4 Cr-1 Mo pressure vessel steel, ASTM A542, Class 3 (hereafter referred to as SA542-3), which is a candidate material for coal conversion applications. A 175 mm thick section plate of the steel (Lukens heat no. 3707) was obtained in the following heat-treated condition: austenitized for 5-1/2 hr. at 954°C, water quenched, tempered for 8 hr at 663°C and stress relieved for 15 hr at 593°C, 22 hr at 649°C and 18 hr at 663°C. Chemical composition and ambient temperature mechanical properties are listed in Tables 1 and 2 respectively. Micro-structures in the plate were fully bainitic with less than 3% free polygonal ferrite at center thickness, with a prior austenite grain size of roughly 70 μm (Figure 2).

For comparison purposes, additional tests were performed on a low strength C-Si pipeline steel, ASTM A 516 Grade 70 (referred to as SA516-70) and an ultrahigh strength Si-modified 4340 steel, 300-M. The SA516-70 steel was tested following normalizing at 900°C and showed a 30% pearlitic/70% ferritic structure, with an average ferrite grain size of approximately 30 μm. The 300-M steel was tested at two strength levels, namely after oil quenching from 870°C and tempering at 300°C and at 650°C (hereafter referred to as 300 M - T 300 and 300 M - T 650). Both structures were fully martenistic with a prior austenite grain size of 20 μm. Chemical composition and mechanical properties are listed in Tables 1 and 2.

2.2 Experimental Procuedures

Fatigue crack propagation experiments were performed with 12.7 mm thick compact specimens machined in the T-L orientation. Plane strain conditions were maintained based on the criterion that cyclic plastic zone sizes did not exceed 1/15 of test piece thickness. Testing was performed on 50kN Instron electro-servo-hydraulic machines operating under load control. Tests were conducted at ambient temperature in moist air (30 pct relative humidity), distilled water, and high purity dehumidified hydrogen and helium gases. Hydrogen and helium atmospheres
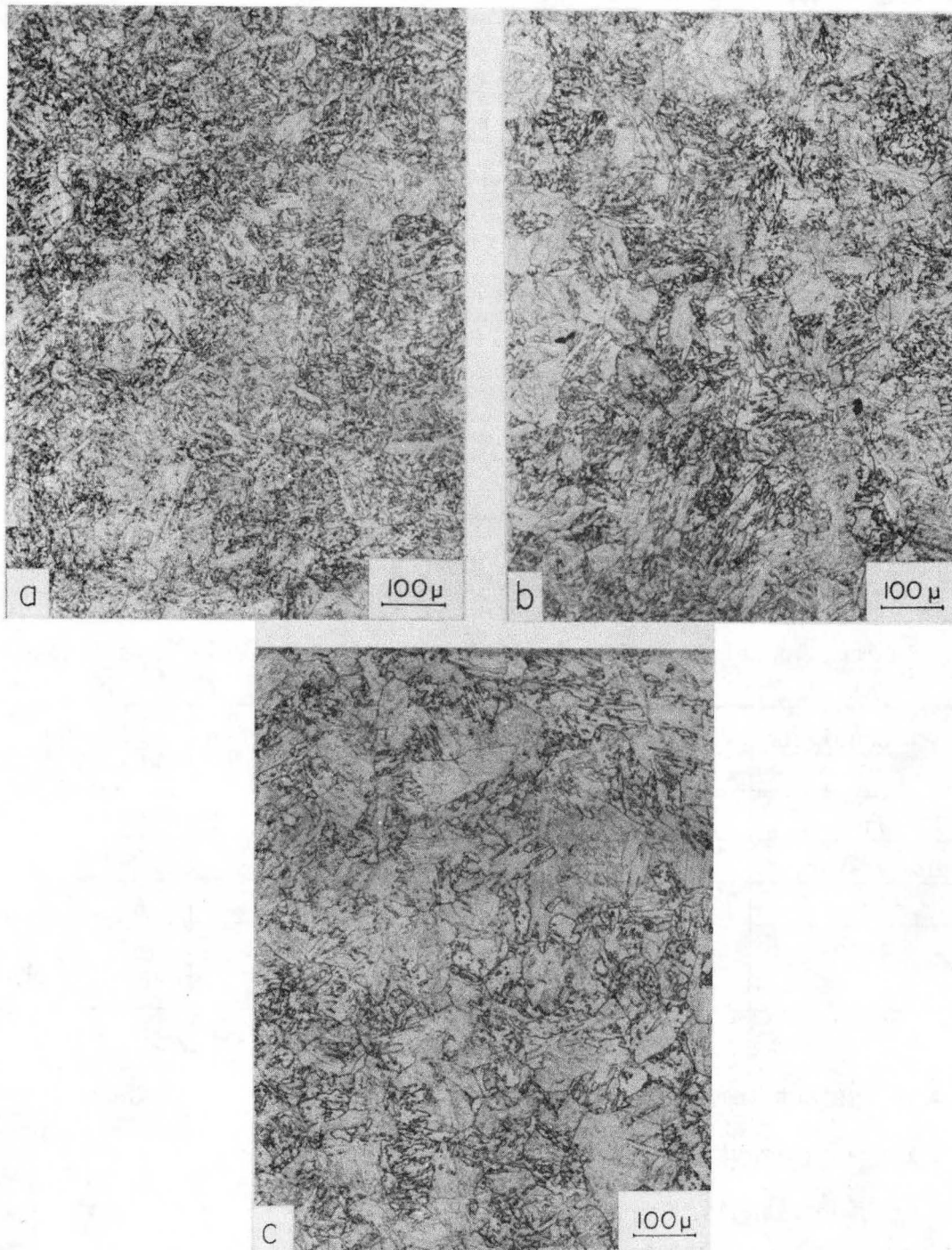
Figure 2. Optical micrograph of SA542 Class 3, 174 mm thick base
plate at a) surface, b) quarter thickness (¼ T), and
c) mid-thickness (½ T) locations (2% nital etch).

TABLE 1

Base Plate Chemistries in wt.% of Steels Investigated

Steel	Type	C	Mn	Si	Ni	Cr	Mo	Cu	P	S	V	Heat Treatment
SA542-3	2¼Cr-1Mo	0.12	0.42	0.25	0.14	2.48	1.06	0.16	0.013	0.020	-	Q & T
SA516-70	C-Si	0.23	1.20	0.25	-	-	-	-	0.006	0.019	-	N
300-M	Ni-Cr-Mo	0.42	0.76	1.59	1.76	0.76	0.41	-	0.007	0.002	0.1	Q & T

Q & T: Quenched and tempered

N: Normalized

TABLE 2

Ambient Temperature Mechanical Properties of Steels Investigated

Steel	Condition	0.2% Proof Stress (MPa)	U.T.S. (MPa)	Elongation (%)	K_{Ic} (MPa$\sqrt{m}$)	K_{Iscc} [1] (MPa$\sqrt{m}$)
SA542-3	as-rec.	500	600	25[2]	295[4]	85
SA516-70	as-rec.	327	496	28[3]	233[4]	-
300-M	T300	1737	2006	12[3]	65	20
300-M	T650	1074	1186	18[3]	152[4]	-

[1] Tests in ambient temperature/pressure hydrogen gas.

[2] On 45 mm gauge length.

[3] On 25 mm gauge length.

[4] Computed from J_{Ic} measurements.

were maintained at 138 kPa pressure in a small O-ring sealed chamber clamped onto the test piece, where gas purity was obtained using an extensive purification system involving molecular sieves, cold traps, and heat bakeable lines (14). Crack growth monitoring was achieved using DC electrical potential techniques capable of detecting changes in crack length of the order of 0.01 mm. Near-threshold growth rates were measured under load-shedding (decreasing stress intensity) conditions, with the threshold ΔK_o defined in terms of a maximum growth of rate 10^{-8} mm/cycle. For decreasing load conditions, at each load level the crack was propagated a distance at least four times the size of the maximum plastic zone size formed at the previous load level. Growth rates above 10^{-6} mm/cycle were measured at constant load amplitude. Full experimental details have been described elsewhere (1, 3, 4).

Characterization of corrosion deposits on fatigue fracture surfaces was performed using a fully computer-controlled PHI Model 550, ESCA/ scanning Auger spectrometer. ESCA studies on fracture surfaces and at 25 $\overset{o}{A}$ depth (after ion sputter-etching) were conducted to identify the nature of the oxides formed. By comparing the resulting ESCA survey spectra with standard spectra, the composition of the surface oxide was deduced. To determine the extent of oxidation, depth composition profiles were obtained as a function of Auger sputtering time, calibrated using a known thickness of tantalum oxide standard. The corresponding rates for iron oxide were estimated using the data on argon ion sputtering yields (atom/ion) from Veeco Brochure V60 and Physical Electronics (15). O and Fe Auger peaks, as well as C peaks, were monitored and their amplitudes measured as a function of sputter time. From this information, an estimate of the thickness of fracture surface oxide debris was obtained. Auger spectroscopy measurements are discussed in greater detail elsewhere (44).

Experiments to measure the rate of hydrogen transport in SA542-3 utilized the electrochemical permeation procedures of Kurkela and Latanision (16), based on the technique developed by Devanathan and Stachurski (17). A schematic diagram of the hydrogen permeation cell used is shown in Fig. 3. The material under investigation is made a bi-electrode in the form of a membrane (about 1.5 mm in thickness) and clamped between the cathode (hydrogen entry) and anode (hydrogen exit) half-cells exposing 1.27 cm of the surface area. An electrolyte

CATHODE SIDE

Ammeter

Gas output

Gas input N_2

O.1N H_2SO_4

Pt counter electrode

solution drain

External resistance

Power supply

Potentiostat

W R A

Dental resin

O-rings

Holder

Luggin probe

Tensile specimen

To the grips of an Instron machine

Electro-meter

Strip chart recorder

Gas output

Gas input N_2

Pt counter electrode

O.1N NaOH

solution drain

ANODE SIDE

Buffer solution O.1N Na_2SO_4

Saturated KCl

Calomel electrode

Figure 3. Hydrogen Permeation Cell

solution of 0.1N H_2SO_4 is used in the cathode half-cell and 0.1N NaOH in the anode half-cell. To minimize the effects of oxygen reduction, both solutions are de-aerated prior to and during the experiment by bubbling nitrogen gas. Hydrogen charging is controlled by a galvano-static circuit which insures that the cathodic charging current is a function of the external resistance and not the cell resistance. Hydrogen is adsorbed into the membrane and diffuses through to the other side. The anodic side of the specimen is maintained at a constant potential versus a saturated calomel electrode by a potentio-stat so that the concentration of hydrogen on that surface is zero. Thus, when hydrogen emerges at the anodic side, it is immediately oxidized and the current generated thereby is a direct measure of the permeation rate. To make sure that the oxidation of hydrogen is the sole reaction, the anodic side is plated with palladium to suppress the oxidation of iron (this has no effect on the permeation behavior). The permeation current is measured by an electrometer and recorded on chart paper. All experiments were carried out at ambient temperatures.

3. REGIMES OF HYDROGEN-ASSISTED CRACKING

3.1 Introduction

Lower strength steels, with yield strength values typically below 1000 MPa, have traditionally been considered to be relatively immune to embrittlement in the presence of hydrogen gas, a notion which has persisted due to their high K_{Iscc} threshold stress intensities for hydrogen-assisted cracking under sustained loading. However, from the initial results obtained in this work on low strength steels, it has become evident that such steels may be susceptible to marked hydrogen-assisted cracking under cyclic loading at stress intensities well below K_{Iscc}. The ambient temperature fatigue crack propagation behavior of SA542-3 is shown in Figs. 4 and 5 for environments of moist air and low pressure dehumidified gaseous hydrogen for a range of frequencies (0.5 to 50 Hz) and load ratios (0.05 to 0.75). Fig. 4 shows the effect of frequency at a load ratio of 0.05, and Fig. 5, the effect of load ratio at a frequency of 50 Hz. It is apparent that there are two regions of fatigue crack propagation where dry hydrogen causes significant increases in crack growth rates compared to moist ambient air, as shown schematically in Fig. 6. The characteristics of hydrogen effects in these regimes are examined below.

3.2 Mid-range of Growth Rates

In the mid-growth regime (crack propagation rates in excess of 10^{-5} mm/cycle), the presence of gaseous hydrogen causes enhancement in growth rates (up to 20 times) compared to air. These accelerations seem to occur at an approximately constant K_{max} value, termed K_{max}^{T} (roughly 20 MP a$\sqrt{m}$ in the present case), i.e. at lower ΔK levels with increasing load ratio (Fig. 5), provided the frequency is below a critical value (dependent on R). However, frequency and load ratio have little effect on the fatigue crack propagation for tests conducted in moist air. Table 3 summarizes the K_{max}^{T} values for different frequencies and load ratios obtained for tests in hydrogen.

The sudden transition to a higher growth rate in hydrogen is observed to result in a change from a predominately transgranular to a predominately intergranular fracture at stress intensity values around K_{max}^{T} as shown in Fig. 7. The characteristic fracture in air, however, is predominately
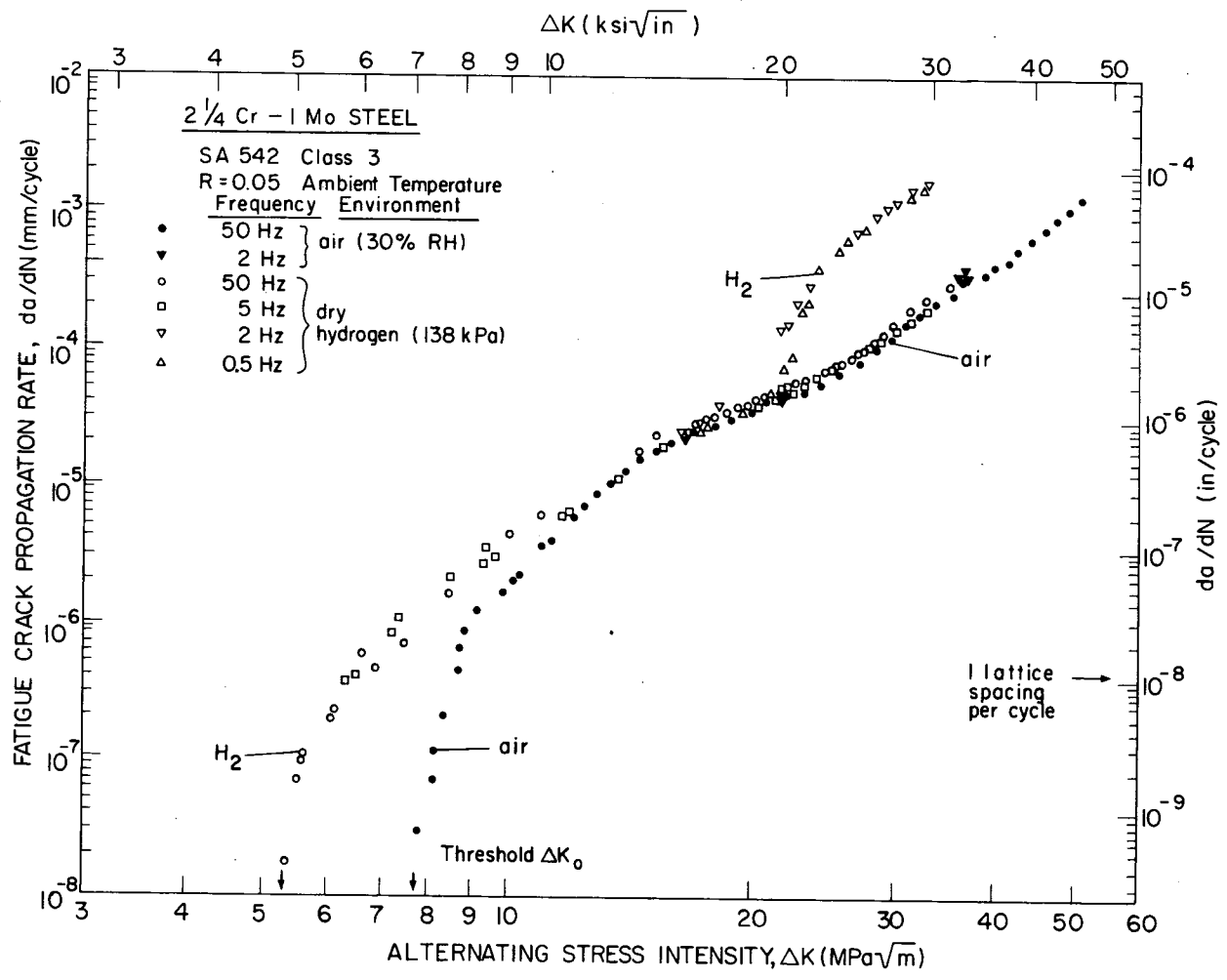
Figure 4. Influence of frequency on fatigue crack growth rate in SA542-3 steel tested at R = 0.05 in moist air and dry hydrogen.
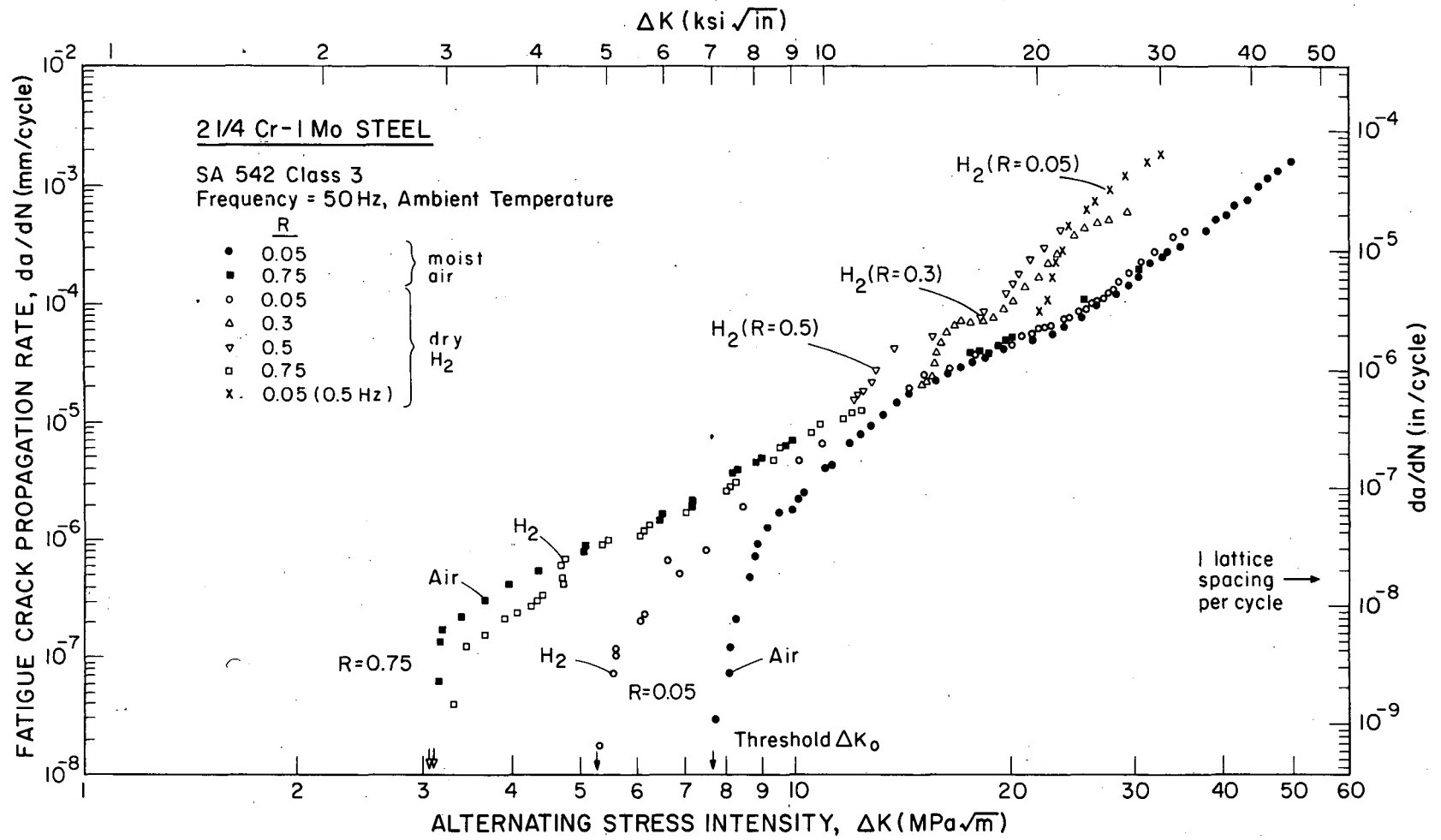
Figure 5.   Influence of load ratio R on fatigue crack growth rate in
            SA542-3 steel tested at 50 Hz in moist air and dry hydrogen.
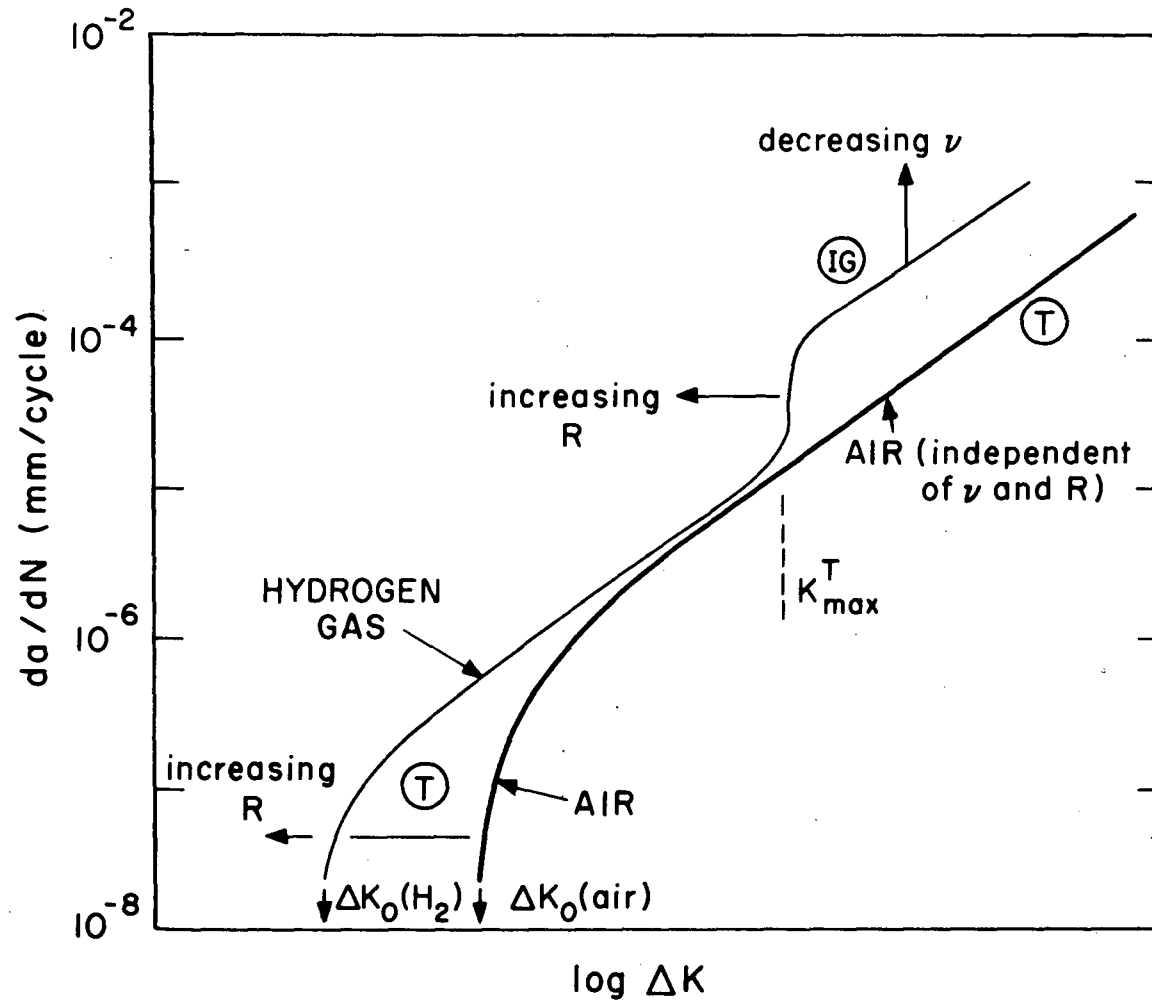
Figure 6. Schematic showing regimes of hydrogen-assisted crack growth commonly observed in lower strength steels.

TABLE 3

Conditions for Onset of Hydrogen-Assisted Crack Growth in SA542-3

R	Frequency	ΔK^T	K^T_{max}
	(Hz)	(MPa$\sqrt{m}$)	
0.05	50	no effect	
0.05	5	no effect	
0.05	2	21.8	22.9
0.05	0.5	21.2	22.3
0.30	50	15.3	21.9
0.30	5	14.4	20.6
0.50	50	11.8	23.6
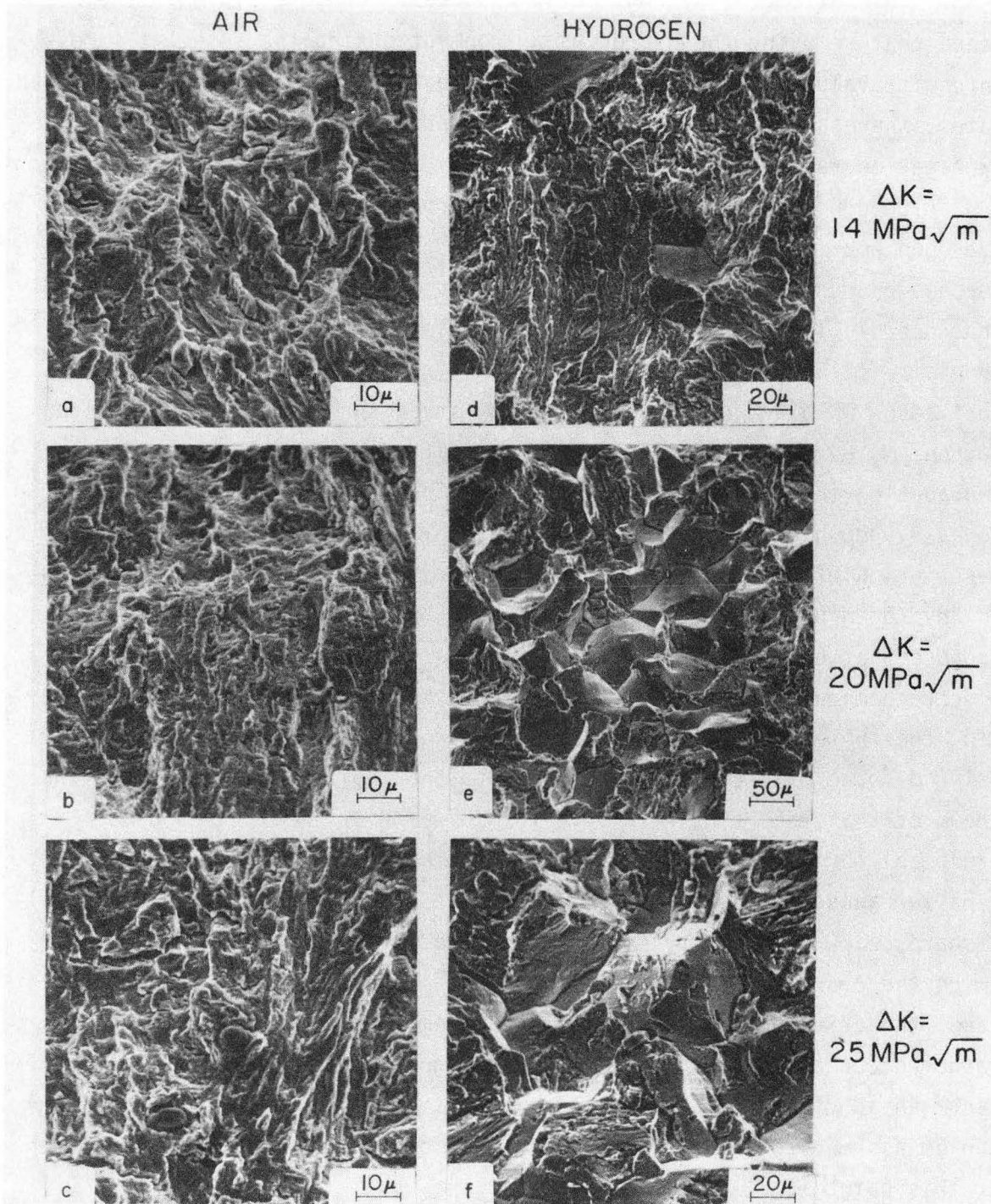
Figure 7. Fractography of fatigue crack growth in 2¼ Cr-1Mo steel at 50 Hz in moist air and dry hydrogen gas (R = 0.03).

AIR

HYDROGEN

$\Delta K = 14\ MPa\sqrt{m}$

$\Delta K = 20\ MPa\sqrt{m}$

$\Delta K = 25\ MPa\sqrt{m}$

XBB 8110-9784

-17-

transgranular with isolated intergranular facets, both below and above K^T_{max}. This effect of hydrogen also appears to be reversible in the sense that removing the hydrogen environment during the test, at stress intensity values above K^T_{max}, results in up to 20 times decrease in growth rates, whereas re-introducing hydrogen leads to an acceleration in propagation rates by a similar magnitude.

Although many mechanisms have been proposed over the years for the hydrogen embrittlement of steels, such as the Pfeil-Troiano-Oriani decohesion models (18) and the Zappfe pressure model (19), it is unlikely that one single theory can provide a complete understanding of the problem. (Since precise mechanisms of hydrogen embrittlement are in most cases unknown, particularly in low strength steels, we imply here mechanisms by which hydrogen enters the lattice and promotes some degradation in resistance to fracture). For high strength steels, however, decohesion theories appear to provide at least a partial description of observed behavior, both for monotonic and cyclic loading in "hydrogen-producing" atmospheres, such as H_2O and H_2S. Such models propose that hydrogen is adsorbed from the gas phase, or evolved by electrochemical reaction (20), on freshly reactive surface at the crack tip, thereby entering the lattice and being transported, under the driving force of the stress gradient, to the region of maximum dilation ahead of the crack tip where some form of embrittlement takes place presumably by a reduction in cohesion at interfaces (Fig. 8). (Unlike behavior ahead of a blunt notch, the point of maximum dilation ahead of a sharp crack may be very close to the crack tip, i.e. of the order of twice the crack tip opening displacement. Accordingly, in this latter case, the critical event involved in the embrittlement process may rather occur at some microstructurally-significant characteristic distance ahead of the crack tip). The reduction in cohesive strength ($\Delta\sigma_H$) can be assumed to be proportional to the local concentration of hydrogen at this point (C_H), where

$$C_H = C_0 \cdot \exp (\sigma \bar{v}/R_0 T) . \qquad (1)$$

C_0 is the equilibrium concentration of hydrogen in the unstressed iron lattice, $\bar{v}$ the partial molar volume of hydrogen in iron, σ the hydrostatic tension, R_0 the gas constant, and T the absolute temperature (21).

σ_{yy}

elastic/plastic
stress distribution

crack tip region

X

gaseous H_2

1

2

3

4

embrittlement
region

5

1. Gas Phase Transport
2. Physisorption
3. Chemisorption (dissociation)
4. Solution in Metal Lattice (hydrogen entry)
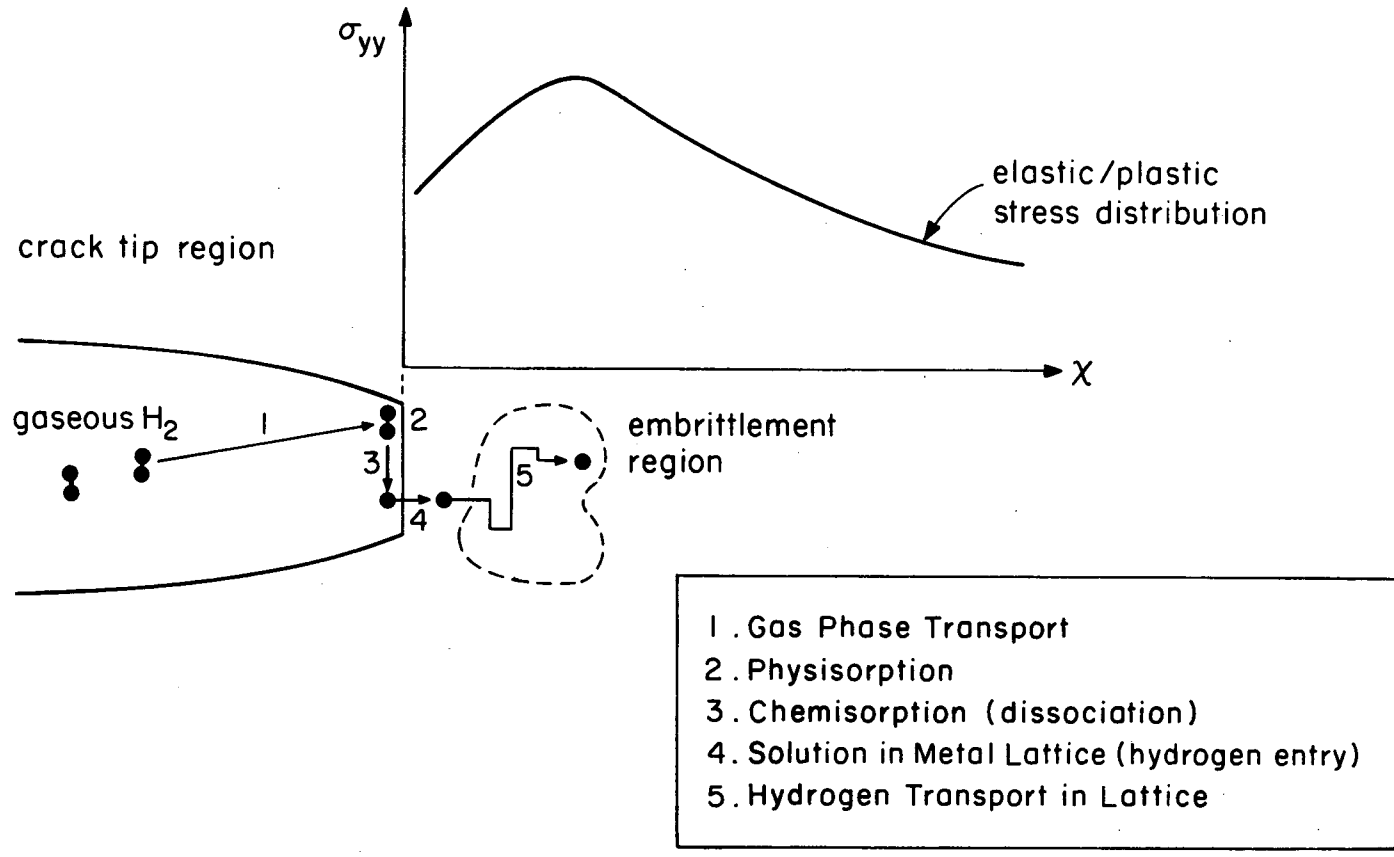5. Hydrogen Transport in Lattice

Figure 8.   Schematic illustration of possible transport processes involved
in the embrittlement of ferrous alloys by gaseous hydrogen
environments.

Such models are consistent with an increasing susceptibility to hydrogen embrittlement with increasing material strength (21), since hydrogen enrichment factors (C_H/C_0) are an exponential function of the hydrostatic tension.

The mechanistic aspects of hydrogen-induced cracking in lower strength steels, on the other hand, are still unclear. Classical decohesion models (18, 21) pose a problem since they predict only marginal enrichment factors due to the small magnitude of the hydrostatic tension in lower strength materials. For external environments, classical pressure models (19), where hydrogen is assumed to accumulate within internal voids in molecular form and exert gas pressures, are also inappropriate since internal pressures cannot exceed the external pressure of hydrogen. Beachem has proposed that hydrogen assists deformation in some unspecified manner and thereby promotes fracture, which is consistent with observations of reduced flow stresses after charging (22). However, the precise interaction between hydrogen atoms and dislocations, although clearly of importance to the embrittlement of iron alloys, remains undefined at this time (23). Recent metallographic studies (24, 25) have indicated that hydrogen may enhance the nucleation and growth of microvoids at internal surfaces in low strength steels, but it is not known whether such "micro-decohesive" mechanisms are important during fatigue, where a complete mechanistic basis for crack growth, even in the absence of environmental effects, is still lacking.

Hydrogen-assisted fatigue crack growth in the low strength bainitic pressure vessel steel is characterized by a marked load ratio/frequency dependence, is coincident with a fracture mode change from predominantly transgranular to intergranular cracking, and occurs above a critical K_{max} value, K_{max}^T, which is small compared to K_{Iscc}. Many authors have observed similar hydrogen-assisted cracking in higher strength steels, with a similar load ratio/frequency dependence, when K_{max} exceeds K_{Iscc} (26-29). The phenomenon, referred to as "stress corrosion fatigue" (Fig. 9b)(26), has been interpreted in terms of a superposition (27) or process competition (28) of sustained load hydrogen-induced cracking and pure mechanical fatigue components. Reaction kinetic studies (20, 30) indicate that such environmentally-induced cracking can be attributed to a mechanism of hydrogen embrittlement, rate-limited by surface reactions
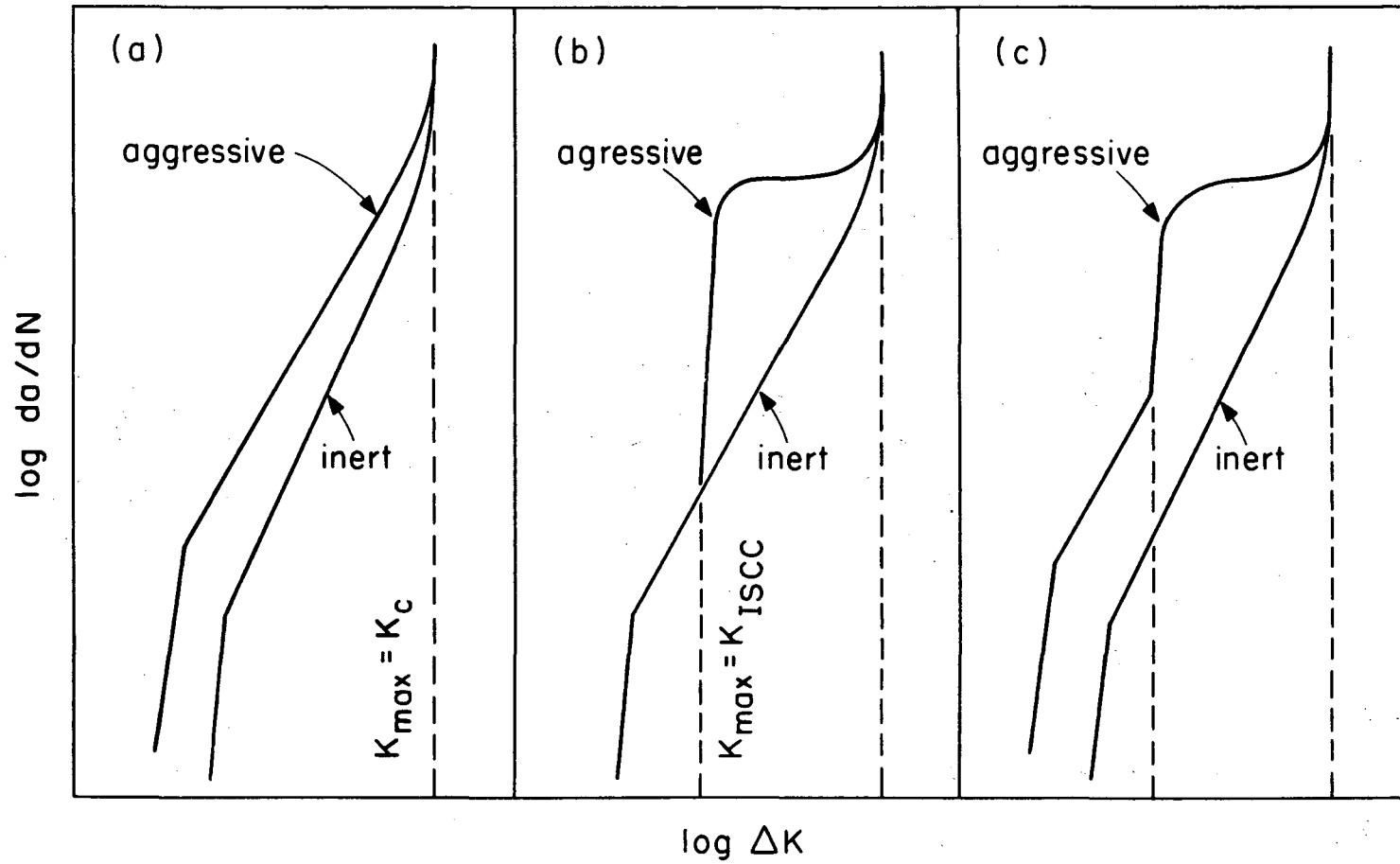
Figure 9.   Basic types of corrosion fatigue crack growth behavior:
            a) true corrosion fatigue; b) stress corrosion fatigue;
            c) s.c.f. and t.c.f. combined (after McEvily and Wei, 1971).

at the crack tip. Specifically, it appears that in gaseous hydrogen
atmospheres this rate-limiting step involves chemisorption of hydrogen
atoms, whereas in water environments, crack growth is limited by the
oxidation of freshly exposed iron surface at the crack tip (20, 30).

Similar kinetic studies (30) in a lower strength steel (SA542-2)
have shown that hydrogen-assisted cracking in this regime (i.e. above
K_{max}^{T}) is also rate-limited by chemisorption for crack growth in gaseous
hydrogen, and the acceleration in growth rates has been attributed to
hydrogen embrittlement mechanisms (although the precise nature of these
mechanisms for lower strength steels are uncertain). In view of the
presence of a predominantly intergranular fracture for hydrogen-assisted
cracking in the present study, it is not unreasonable to presume that
the embrittlement mechanism involves hydrogen-induced decohesion at
grain boundaries, similar to that observed in high strength steels (18).

In terms of macroscopic growth rate behavior, the data in Figs. 4
and 5 indicate that an effect analogous to stress corrosion fatigue takes
place in the mid-growth rates above 10^{-6} mm/cycle) in lower strength
steels, with the very notable exception that it occurs at stress inten-
sities well below K_{Iscc}, i.e. at $K_{max}^{T} > K_{Iscc}$ where no such hydrogen
embrittlement would normally result under purely sustained loading.
This suggests some synergistic interaction (rather than additive or
mutually-competitive interactions) between environment and mechanical
fatigue contribution to crack growth. However, rather than occurring
through some basic change in embrittlement mechanism, it is felt that
the role of cyclic loading is simply to maintain a sharpened crack tip,
thus continuously providing freshly exposed metal surface there for
hydrogen to adsorb.

One is now faced with a terminology problem since the nature of the
hydrogen-assisted growth observed, with its characteristic fracture mode
and frequency/load ratio dependence, conforms to stress corrosion fatigue
(c.f. Fig. 4 with Fig. 9b), yet in lower strength steels the effect
clearly occurs "below K_{Iscc}". Conventionally, such environmentally-
assisted fatigue behavior below K_{Iscc} has been termed "true corrosion
fatigue" (26, 31, 32), as shown in Fig. 9a, yet the characteristics of
the present effect clearly differ from those depicted in this figure.
It is apparent that the commonly used "above and below K_{Iscc}" terminology

(26, 31, 32) for corrosion fatigue, whilst perhaps providing simple and useful classification for strain-rate insensitive high strength steels, can be misleading for lower strength materials. This follows from the fact that in such ductile alloys, the stress intensities necessary for the onset of such hydrogen-induced cracking (from hydrogen embrittlement) are different under sustained and cyclic loading (i.e. $K_{Iscc} \neq K_{max}^{T}$). Two reasons can be provided for this. First, as pointed out for aqueous corrosion fatigue by Ford (33) and Dawson and Pelloux (34), lower strength steels are more strain-rate sensitive compared to high strength steels such that K_{Iscc} environmental thresholds should not be taken as material constants for a particular alloy/environmental system, and can be expected to be reduced under dynamic (i.e. cyclic) straining conditions. Second, since K_{Iscc} measurements are often performed on test pieces previously pre-cracked in air, and stressed under fixed-load or rising-load conditions, the critical event for determining the K_{Iscc} threshold may often simply involve hydrogen permeation through, or fracture of, the protective oxide scale previously formed at the crack tip. In fact, by pre-cracking in the actual hydrogen environment under test and employing fixed displacement conditions on side-grooved specimens, Shaw (35) has recently demonstrated that significantly lower K_{Iscc} values, approaching K_{max}^{T} values, can be measured in lower strength steels including 2¼ Cr-1Mo alloys.

Thus, it is reasonable to regard the value of K_{max}^{T} as an effective threshold stress intensity in fatigue for gaseous hydrogen-induced cracking by hydrogen embrittlement mechanisms (similar to the mechanism under sustained loading), which is nominally equal to the sustained load K_{Iscc} threshold in strain rate-insensitive high strength steels (26), yet is considerably less than K_{Iscc} in the present lower strength steels. (The role of hydrogen in influencing fatigue crack growth at near-threshold levels is considered to be largely independent of conventional hydrogen embrittlement mechanisms as discussed in Section 3.3).

Similar arguments (33, 34) have been proposed for corrosion fatigue crack growth for the mid-growth regime in aqueous environments for a number of alloy systems, where the environmental contribution to cracking involves active path corrosion in addition to, or in place of, hydrogen

embrittlement mechanisms. Dawson and Pelloux (34), in fact, refer to their environmental threshold as ΔK_{scc} for aqueous corrosion fatigue in titanium alloys. However, since the onset of the environmentally-assisted crack growth occurs above a constant maximum stress intensity (K_{max}^T)(independent of R), for the present case of gaseous hydrogen environments (Table 3), it is preferable to define the environmental threshold in terms of a K_{max} value, rather than a particular alternating stress intensity. It is perhaps worth noting here that certain authors (2, 36-39), who have examined fatigue crack propagation behavior over a limited range of growth rates, have mistakenly interpreted this environmental threshold as the ΔK_o threshold for no fatigue crack growth. As shown by the data in Figs. 4 and 5, this is clearly erroneous, since ΔK_o thresholds are generally an order of magnitude smaller.

Finally, the question arises as to the reason for the existence of an environmental threshold stress intensity (K_{max}^T) for a hydrogen embrittlement contribution to fatigue crack growth. From the present data, the value of K_{max}^T appears dependent upon frequency (Figs. 4 and 5) and hydrogen pressure (discussed later in this Section), and independent of load ratio (Table 3). Such observations are consistent with modelling studies (18, 21) which equate the critical stress intensity above which hydrogen embrittlement is predominant with a critical solubility of hydrogen ahead of the crack tip. From Eq. 1, this critical hydrogen concentration (C_H) is dependent upon the hydrostatic stress and the hydrogen concentration in the lattice. Thus, by increasing the hydrogen pressure, an earlier onset of hydrogen-assisted growth is to be expected, whereas the similar effect observed with decreasing frequency (Fig. 4) is at least qualitatively consistent with the kinetic aspects of there being sufficient time for the critical step in the hydrogen embrittlement process to occur. This critical step can be considered in terms of the competition between several processes (Fig. 8), principally involving the rate of hydrogen adsorption at the crack tip, its transport into the lattice, and the rate of formation of fresh surface as the crack grows. Of these, hydrogen transport can be quickly dismissed as a rate-limiting step simply from hydrogen diffusion data. Using the electro-chemical permeation technique of Devanathan and Stachurski (17), our measurements on unstressed samples of SA542-3 yielded a diffusion coefficient for

hydrogen permeation (D) of roughly 5×10^{-7} cm^2/sec. Using the simple relation for the distance x for hydrogen diffusion into the lattice in time t, namely,

$$x \sim 4 \sqrt{Dt} \qquad (2)$$

implies that hydrogen will permeate through the lattice by distances roughly 4 and 40 μm during one cycle, for frequencies of 50 and 0.5 Hz, respectively. Since this is several times larger than the crack advance per cycle, and futhermore, actual diffusion rates may be in excess of this due to dislocation aided transport (23, 40) in stressed samples, hydrogen transport can clearly not be considered as rate-limiting for the frequency range studied. However, as noted above, more detailed kinetic studies by Wei and co-workers (20, 30) equate the rate-limiting step to chemisorption of hydrogen at the crack tip for gaseous hydrogen atmospheres. Related arguments have been advanced for the analogous effect of an environmental threshold for corrosion fatigue in aqueous environments, where the frequency dependence on K^T_{max} is assumed to be a function of the interaction between the rate of oxide rupture at the crack tip, the rate of passivation and the rate of metal dissolution or hydrogen production at the bared surface (33, 34, 41).

3.2.1 Hydrogen Assisted Cracking in SA516-70 Steel

Fig. 10 shows the variation of crack growth rate with stress intensity range for SA516 pipeline steel in environments of moist air and low pressure (0.14 MPa) dry hydrogen gas at load ratios of 0.15 and 0.75. Fatigue data of this steel obtained by Wachob and Nelson (37) in high pressure (6.9 MPa) hydrogen are also plotted in Fig. 10. It is observed that similar to the behavior observed in the case of SA542-3, the pipeline steel also undergoes significant accelerations in propagation rates in the two regions of crack growth, namely, the mid-growth and the threshold regimes.

In the mid-growth region, the crack growth data obtained in the present study, as well as by Wachob and Nelson (37), for environment of moist air are found to be similar. The difference in the testing frequency in the two studies does not appear to result in any significant differences in fatigue behavior. (This and the information on the influence of low pressure hydrogen imply that the critical frequency for any effect of low pressure hydrogen in the mid-growth regime is below 0.1 Hz). It can be

-25-

ΔK (ksi √in)

10⁻² ... see axis

FATIGUE CRACK PROPAGATION RATE, da/dN (mm/cycle)

SA 516 Grade 70 Pipeline Steel

Ambient temperature

	R	Environment	Reference
△	0.15	moist air (30% RH)	present study
○	0.75		(50 Hz)
○	0.15	dry hydrogen (0.14 MPa)	present study
□	0.75		(50 Hz)
▲	0.15	laboratory air	Wachob and Nelson
●	0.15	dry hydrogen (6.9 MPa)	(0.1 - 10 Hz)

high pressure
H₂ (0.15)

low pressure
H₂ and air (0.15)

I lattice
spacing
per cycle

H₂ & air
(0.75)

H₂ (0.15)

△—air (0.15)

△ Threshold ΔK₀

da/dN (in/cycle)

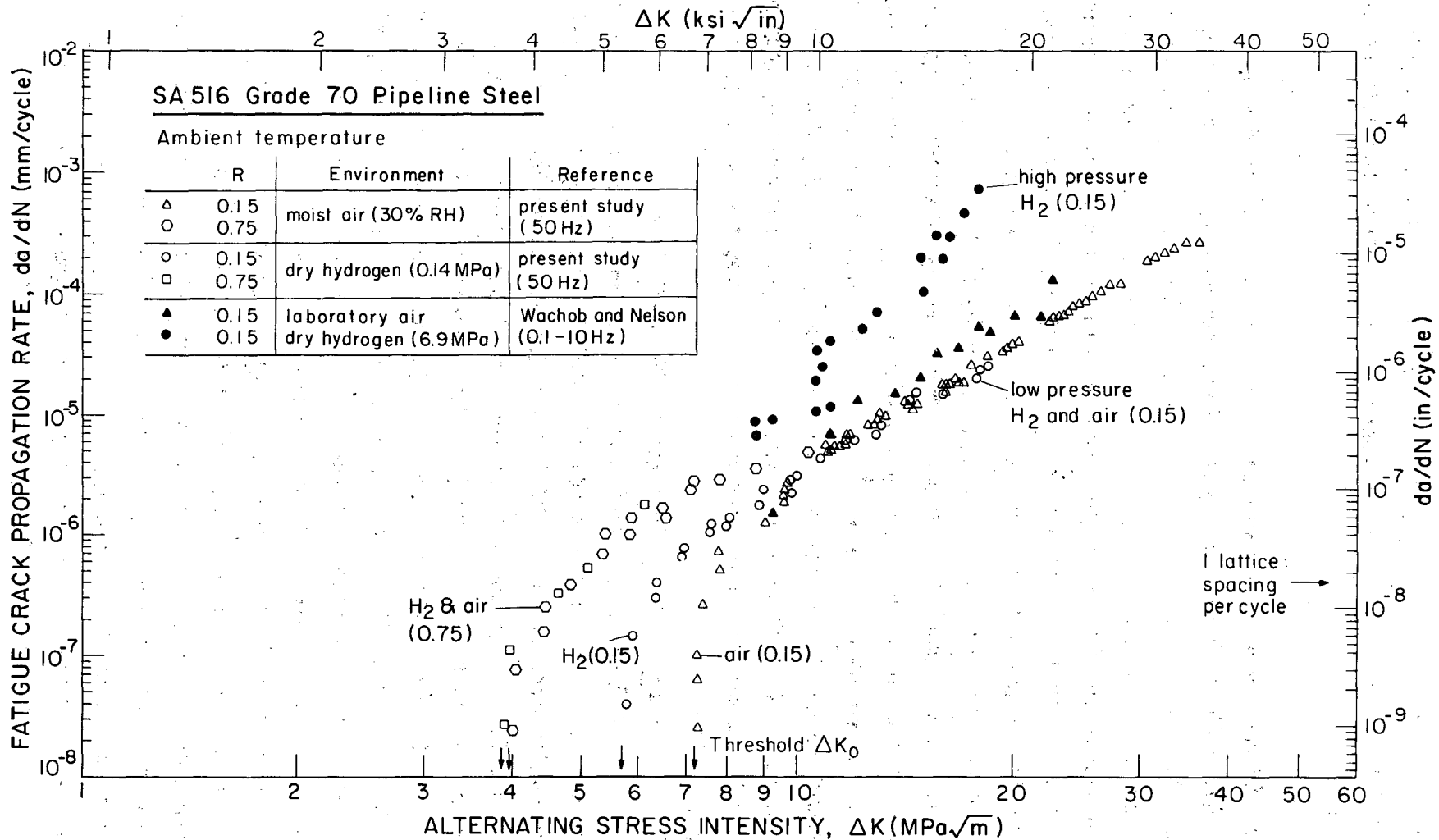**ALTERNATING STRESS INTENSITY, ΔK (MPa√m)**

Figure 10. Fatigue crack propagation in ferritic-pearlitic SA516-70 steel
at R = 0.15 - 0.75 in moist air and hydrogen gas, showing influence
of high pressure (6.9 MPa) hydrogen. (closed symbols refer to data
from ref. 37).

inferred from these results that increasing the pressure of hydrogen from 0.14 MPa to 6.9 MPa leads to considerable acceleration in crack growth rates with a relatively low K_{max}^T value of 11 MPa$\sqrt{m}$ (compared to a K_{max}^T of about 20 MPa$\sqrt{m}$ for low strength SA542-3). This effect of pressure is consistent with the previously presented argument (Section 3) that the influence of hydrogen in accelerating crack velocities at growth rates above 10^{-5} mm/cycle is due to a hydrogen embrittlement mechanism.

In the threshold regime for crack growth, the environmental influences seen in the case of SA516 are similar to those in SA542-3 for both low and high load ratio values. Also, comparison of the results obtained on SA516 in the present study and in Ref. 37 shows no variation in crack growth rate with a change in frequency from 0.1 to 50 Hz above a growth rate of 10^{-6} mm/cycle. Unfortunately, information on crack growth rates near-threshold for high pressure hydrogen or frequencies lower than 50 Hz are not available for SA516.

3.3 Near-Threshold Growth Rates

In the near-threshold regime of crack propagation, where growth rates are smaller than 10^{-6} mm/cycle, increasing the load ratio results in a decrease in threshold ΔK_o up to a certain load ratio value, beyond which it is load ratio-independent, as shown in Fig. 11 for SA542-3 tested moist air environment over a range of R values from 0.05 to 0.75. The most pronounced effect of hydrogen on crack growth is seen in the near-threshold regime, where the presence of dry gaseous hydrogen enhances the fatigue crack propagation rates by up to two orders of magnitude and decreases the threshold stress intensity range by up to 30% compared to moist air. This significant influence of hydrogen is observed only at low load ratios; there is little difference between near-threshold growth rates in air and hydrogen at high R values (Fig. 12). A similar result can be seen for SA516-70 steel, as shown in Fig. 10. The role of dehumidified helium gas at lower growth rates compared closely with that of hydrogen (Fig. 13). Although at the mid-range of growth rates, crack propagation is expectedly slower compared to moist air, at near-threshold levels the presence of the dry inert gas actually accelerates growth rates by over an order of magnitude compared to moist air, the threshold ΔK_o in moist air being 24% higher compared to helium. In contrast,
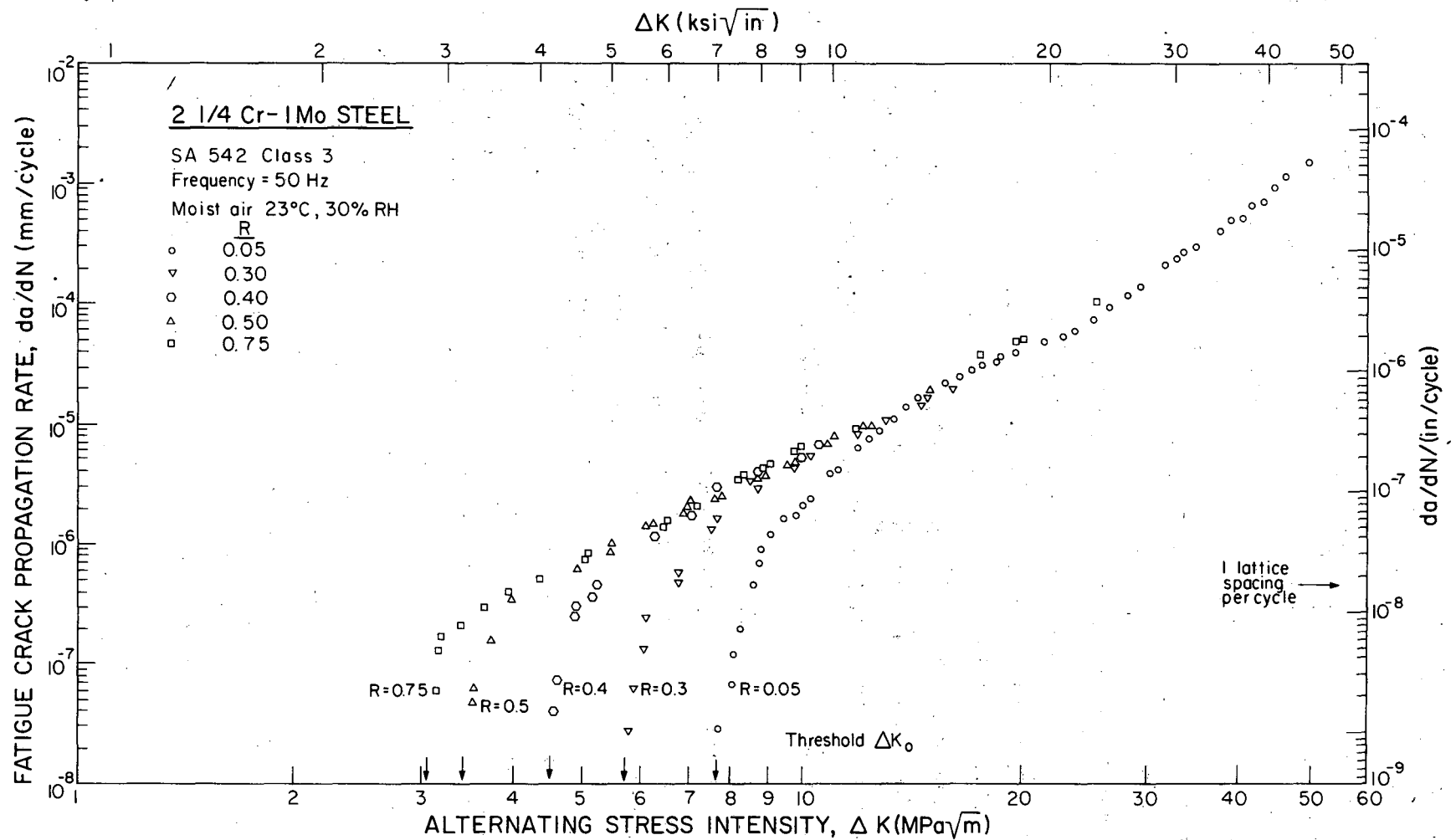
Figure 11. Effect of load ratio on the near-threshold fatigue behavior of SA542-3 steel.
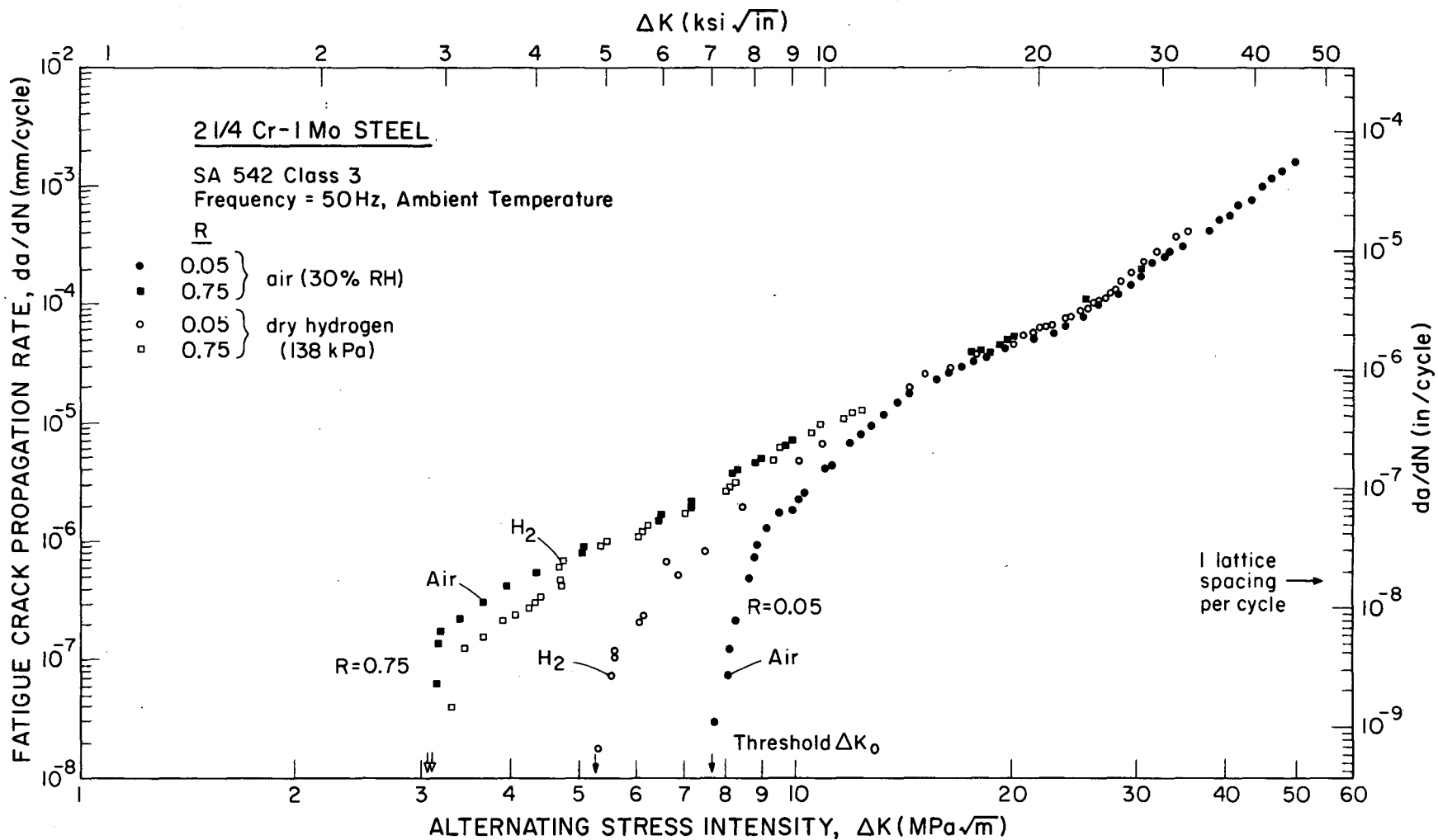
Figure 12. Fatigue crack propagation in SA542-3 steel tested at R = 0.05 and 0.75 (50 Hz) in moist air and dry hydrogen.
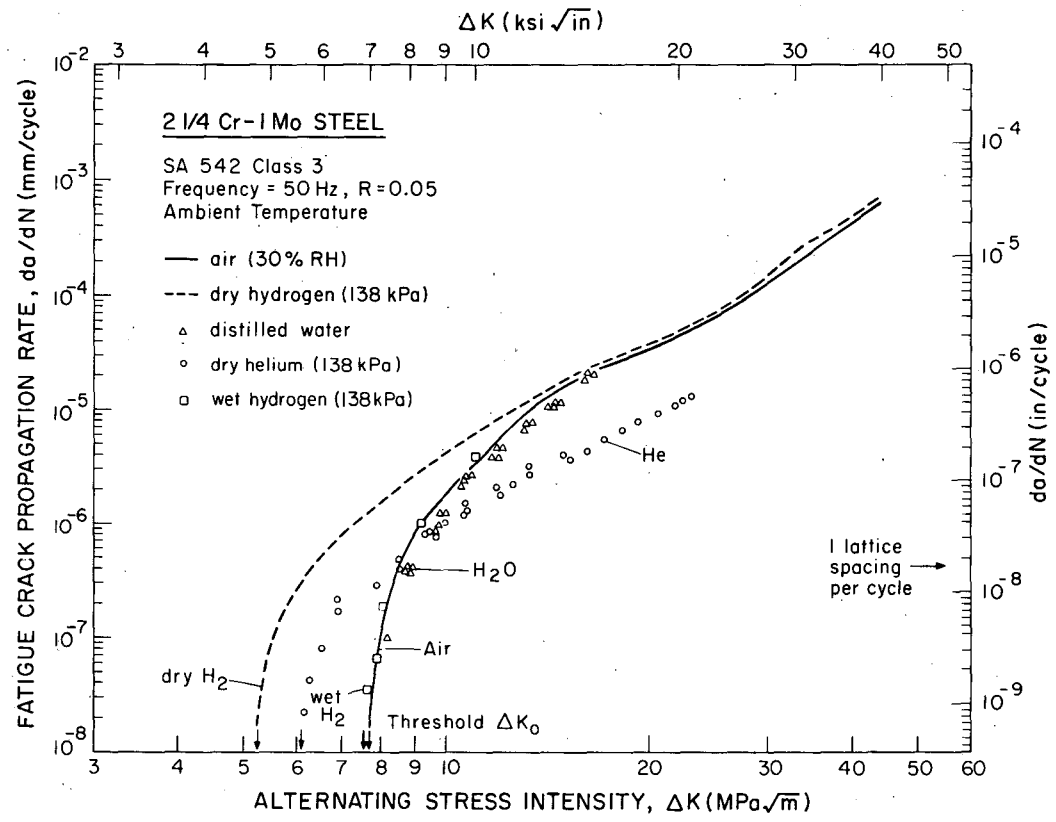
Figure 13. Fatigue crack propagation in bainitic SA542-3 steel tested at R = 0.05 in environments of moist air, water, dry and wet hydrogen and helium.

distilled water environments lead to a marginal deceleration in near-threshold crack growth rates, with a threshold ΔK_0 value fractionally above that measured in humid air, whilst wet hydrogen results in threshold behavior similar to that of moist air (Fig. 13). At such low stress intensities, the fracture mode is predominantly transgranular with evidence of some intergranular separation (Fig. 14). The proportion of intergranular facets, which are not seen at R = 0.75, increases with increasing ΔK to a maximum of typically 30-40% at $\Delta K \stackrel{\sim}{\sim} 15$ MPa$\sqrt{m}$, before decreasing to zero above $\Delta K = 20$-25 MPa$\sqrt{m}$ in air, water, and hydrogen environments*. Little evidence of such facets was seen in helium tests.

The significant influences of hydrogen near threshold have been interpreted previously in terms of hydrogen embrittlement mechanisms (1, 4). Although conventional corrosion fatigue mechanisms (i.e. in the case of hydrogen environments, hydrogen embrittlement mechanisms) have been suggested earlier, the exact nature of such mechanisms had not been explained. In the present work, it has become obvious that such models are not totally consistent with the near-threshold data observed and with the existing data in the literature.

First, although there is a significant influence of hydrogen at low load ratios near threshold, there is little effect of hydrogen at high load ratios. Existing models based on hydrogen embrittlement are not consistent with hydrogen-assisted growth only at low load ratios.

Second, the accelerations in ultra-low crack growth rates in the presence of hydrogen are not accompanied by any apparent change in fracture mode, as was seen in the mid-growth regime. At low load ratios, near-threshold growth rates are similar in hydrogen and helium where the proportion of intergranular fracture is different, whereas the proportion of intergranular fracture is similar in air and hydrogen where the growth rates are different (Fig. 13).

Third, accelerated crack growth rates, compared to moist air, are seen only in dry gaseous hydrogen and dry gaseous helium, whereas rates in wet hydrogen and distilled water are similar to those in air.

The above observations clearly question the role of conventional corrosion fatigue mechanisms, such as hydrogen embrittlement and active

---

*These observations pertain to tests at 50Hz where no abrupt accelerations due to hydrogen, of the nature discussed in Section 3.2, are observed.

AIR   HYDROGEN

HELIUM   WATER

10μm   50μm

10μm   20μm
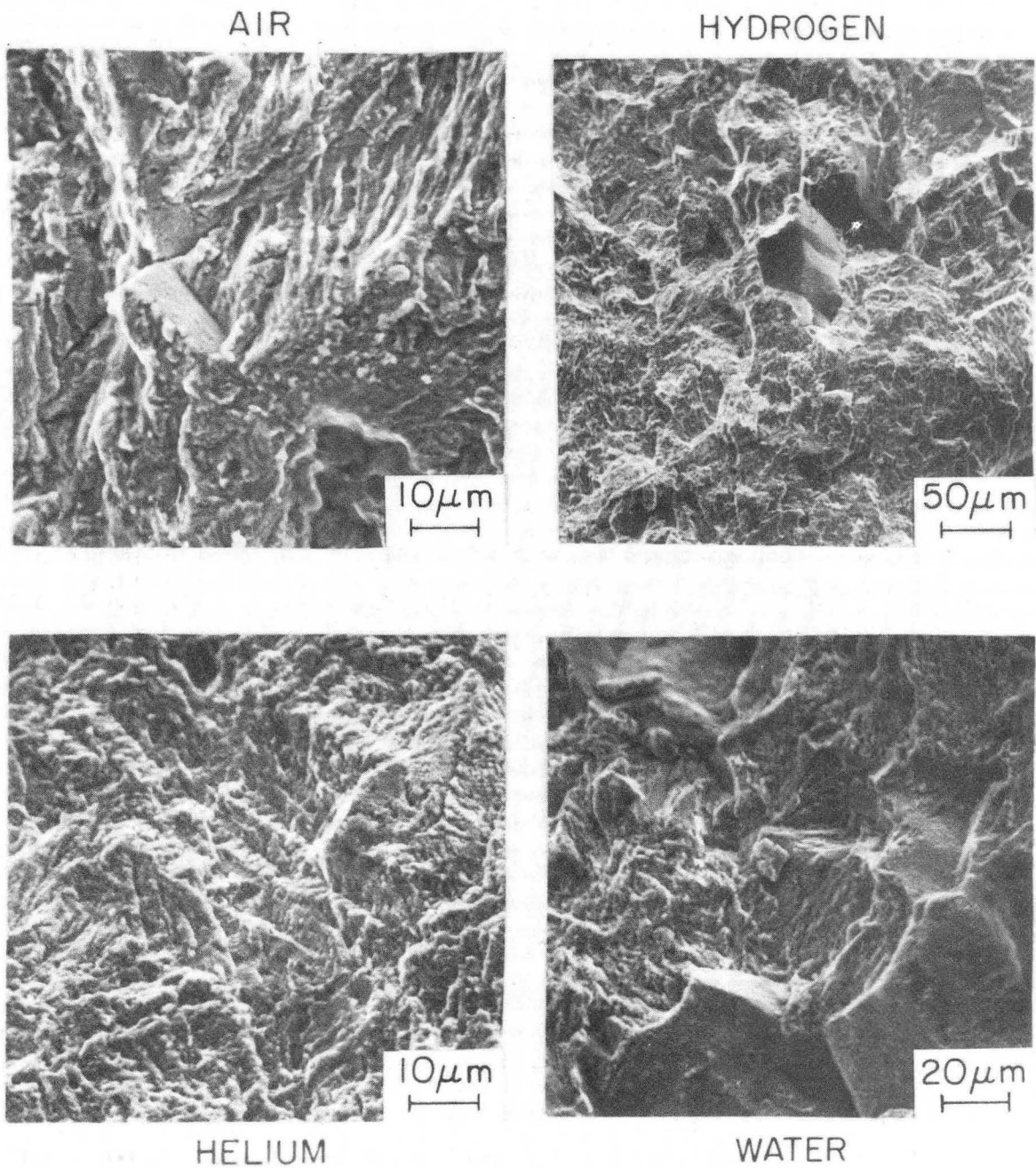
Figure 14.   Fractographs of near-threshold fracture surfaces of SA542-3
steel from tests in air, water, dry hydrogen and dry helium
environments.

path corrosion (metal dissolution), in influencing environmentally-affected near-threshold crack growth. Whilst, it is premature to rule out such mechanisms in actively contributing to behavior, it is apparent that some other mechanism is dominant at such low stress intensities. In the following section, a new model for environmental behavior is presented based on the role of crack tip corrosion deposits in promoting fatigue crack closure. This concept, termed "oxide-induced crack closure", is shown to be consistent with the observed behavior in lower strength steels presented above.

4. A MECHANISM FOR NEAR-THRESHOLD ENVIRONMENTAL EFFECTS IN LOWER STRENGTH STEELS

4.1 Introduction

As discussed in the previous section, it is apparent that whereas conventional corrosion fatigue mechanisms, such as those involving hydrogen embrittlement, may offer viable mechanistic explanations for the role of environment at higher growth rates (typically above $\sim 10^{-5}$ mm/cycle), such mechanisms clearly do not totally describe behavior in lower strength steels at near-threshold levels. Although it is likely that hydrogen embrittlement processes are still occurring, it is clear that the observed behavior is dominated by other processes. In the following sections, a new model is presented based on crack closure originating from oxide debris formed on the crack surfaces. The mechanical and environmental factors influencing near-threshold fatigue behavior, discussed in the previous section, are then rationalized in terms of this oxide-induced crack closure concept.
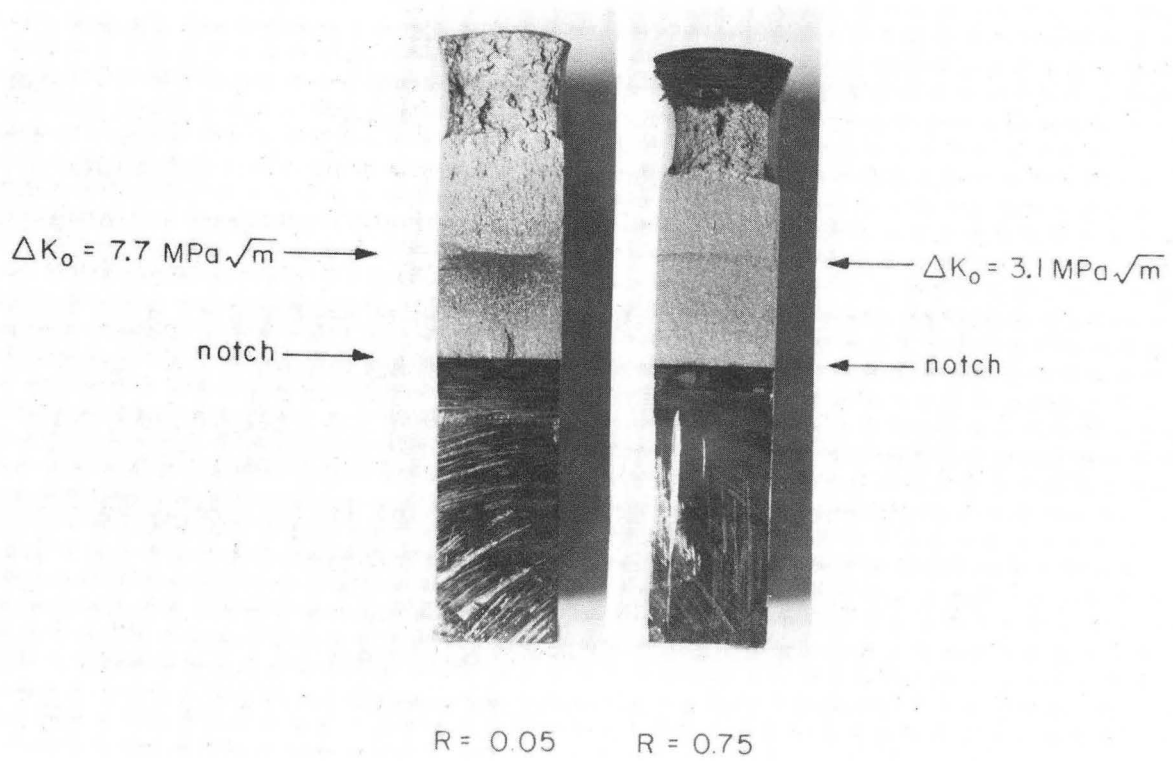
During fatigue crack growth, material is plastically strained at the crack tip, and due to the restraint of surrounding elastic material on this residual stretch, some closure of the crack faces may occur at positive loads of the loading cycle (45). The result of this is a reduction in the stress intensity range, responsible for crack propagation, from a nominal value ΔK ($= K_{max} - K_{min}$) to an effective value, ΔK_{eff} ($= K_{max} - K_{c\ell}$), where $K_{c\ell}$ is the stress intensity to close the crack. However, as the load ratio is raised, the crack remains open for a larger portion of the loading cycle and the effective stress intensity range approaches the nominal value. This phenomenon by which crack tip stress intensity range values are reduced due to a residual stretch and associated contact of fracture surfaces is known as crack closure, or in our terminology, "plasticity-induced crack closure" (42, 44-46).

Although it has long been known that the role of crack closure in the near-threshold regime of crack growth could be quite significant (1, 47), no detailed study of the phenomenon has been carried out. The problem has been that plasticity-induced crack closure is promoted by

plane stress conditions (1) yet at near-threshold levels, plane strain conditions invariably are present. It has become apparent in this study, however, that other mechanisms of crack closure, involving the role of foreign debris and fracture surface roughness, are significant at the very low crack tip displacements associated with near-threshold stress intensities. The mechanism involving enlarged corrosion debris on the crack flanks, in particular, is felt to be responsible for influencing much of the near-threshold corrosion fatigue behavior observed.

Fracture surfaces of specimens which have undergone near-threshold testing are generally characterized by bands of corrosion deposits. Macroscopic examination of such surfaces reveals that the deposits are visually thickest for tests in moist environments at low load ratios, and to be absent for tests at high load ratios at high growth rates (Fig. 15). Comparison of information obtained from X-ray photoelectron spectroscopy (ESCA) analysis with standard spectra for iron oxides show that deposits present on the surfaces are predominantly Fe_2O_3 (Fig. 16). Actual oxide thickness measurements, as a function of crack length (and thus a function of growth rate) are shown in Fig. 17, estimated using Ar^+ sputtering analysis in the Auger spectrometer.

It is apparent that the oxide thicknesses are inversely related to the crack growth rate, and are at a maximum close to ΔK_o. In moist air the maximum thickness is of the order of 0.2 μm at R = 0.05, compared to less than 0.1 μm in hydrogen. (Even after intensive purification of gas streams some residual traces of moisture remain in the system which, aided by a fretting mechanism, result in some oxide formation in dehumidified environments). At R = 0.75, oxide thicknesses in either environment are an order of magnitude smaller. It is also found that the background oxide deposits obtained by exposing a freshly bared surface of the same material to the same laboratory air environment for the same length of time as the duration of a threshold test are roughly 50 Å to 150 Å in thickness which is similar to the amount of oxide formation at higher growth rates. Clearly, the substantial oxide formation at near-threshold stress intensities at low load ratios results from some aspect of the fatigue process. This process has been described as "fretting oxidation", where plasticity-induced crack closure (45) and Mode II displacements (48) lead to abrasion, fracturing and compacting of the

$\triangle K_o = 7.7\ MPa\sqrt{m} \longrightarrow$

$\longleftarrow \triangle K_o = 3.1\ MPa\sqrt{m}$

notch $\longrightarrow$

notch $\longleftarrow$

R = 0.05   R = 0.75

XBB 8110-9786

Figure 15.   Bands of corrosion deposits visible on near-threshold fatigue
             fracture surfaces tested in moist air at   a) R = 0.05 and
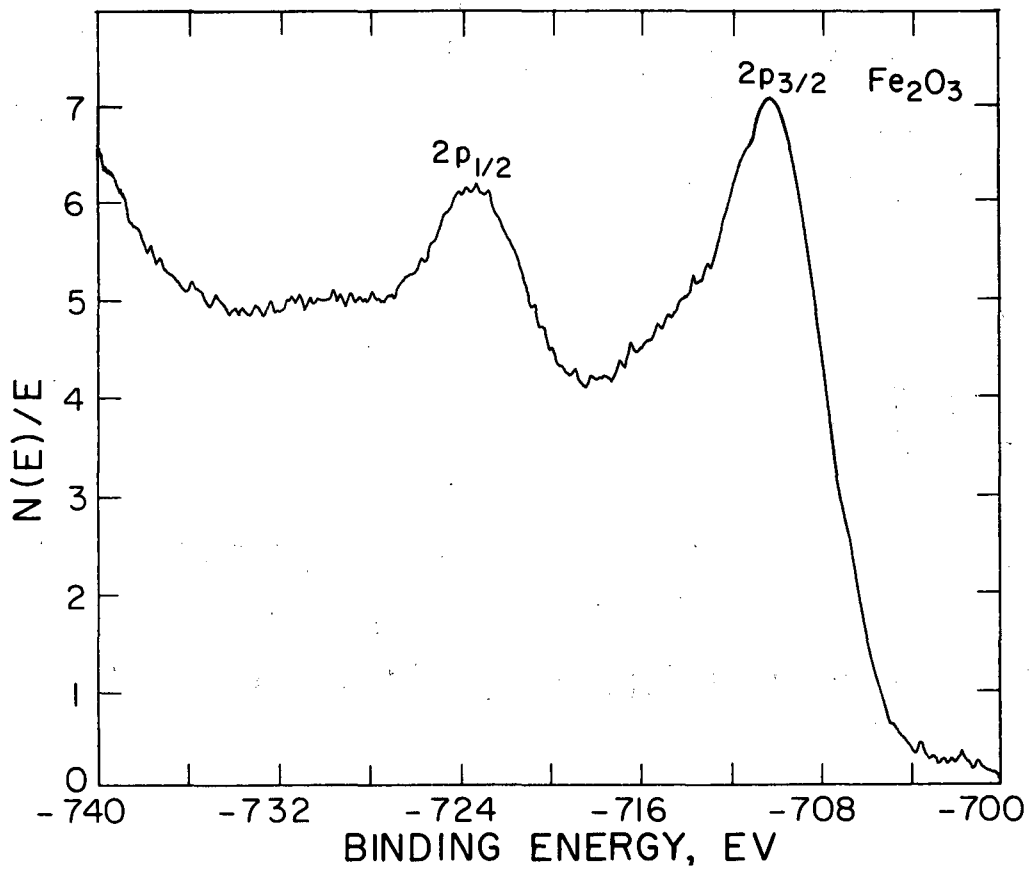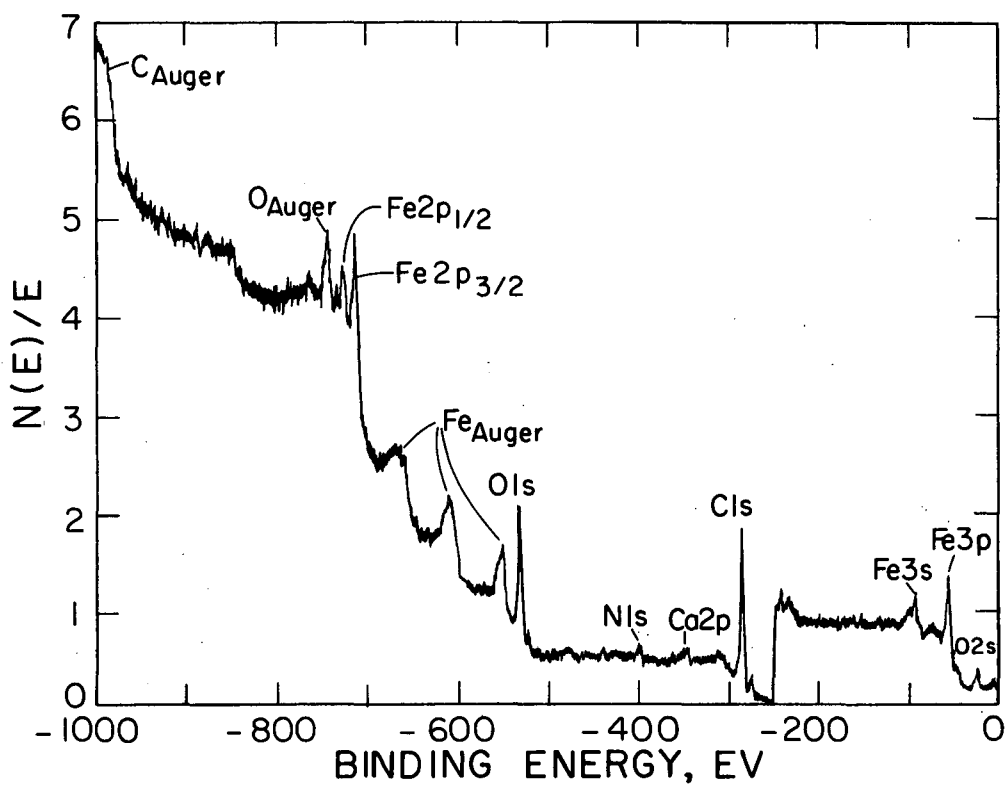   b) R = 0.75.

Figure 16.   ESCA analysis of crack tip corrosion debris in SA542-3 steel showing the presence of predominately Fe_2O_3.
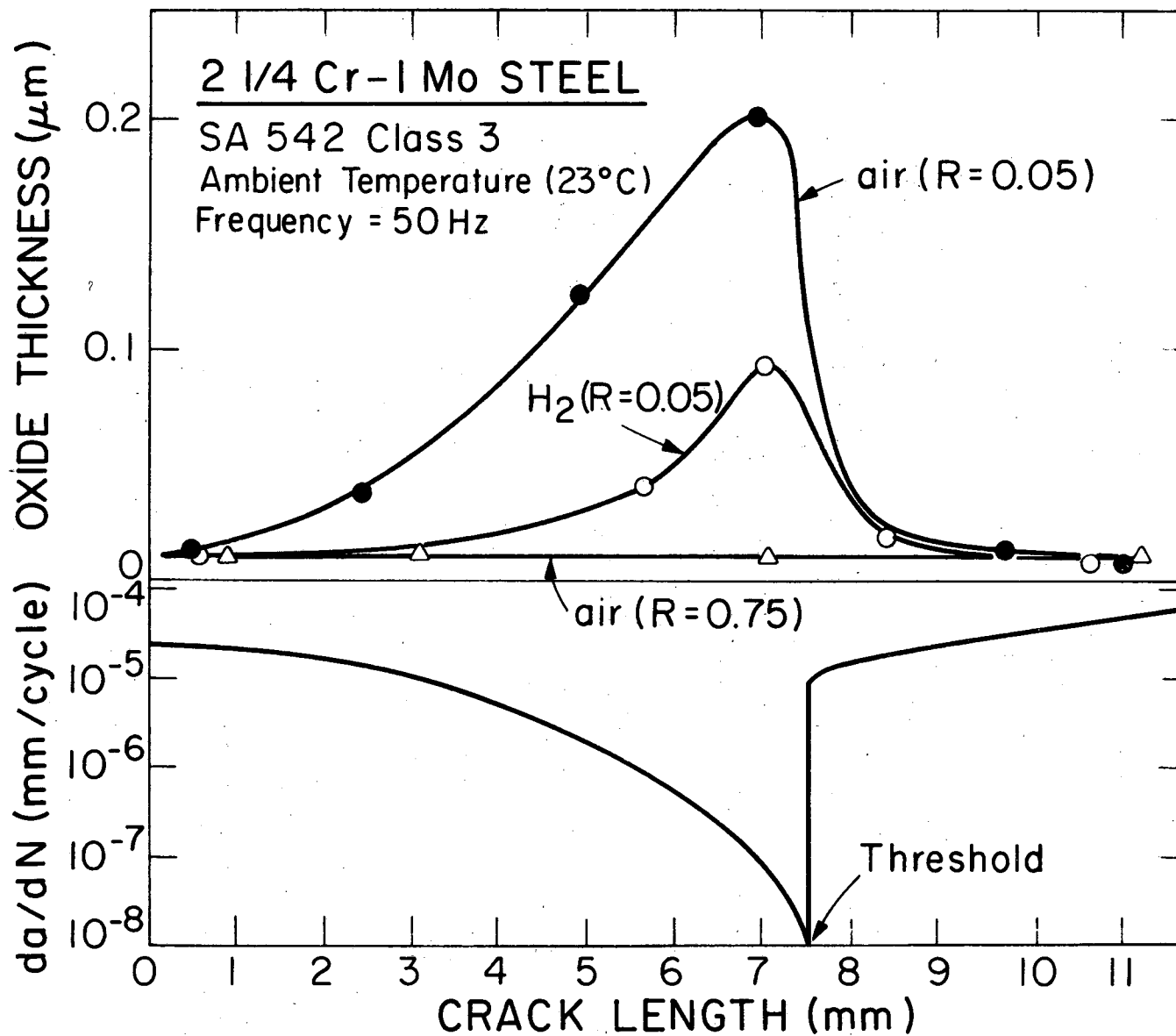
Figure 17. Measurements of oxide thickness as a function of crack length and crack growth rate for SA542-3 steel tested in moist air and hydrogen gas at R = 0.05 and 0.75.

oxide scale at low load ratios, to yield local heating, new zones of exposed surface and hence more oxidation (44, 49). The lack of visible corrosion deposits at high load ratios and at higher growth rates (Fig. 15) is certainly consistent with this mechanism.

4.2 Model for Crack Closure

The significance of oxide layers in promoting crack closure, where cyclic crack tip displacements are small, i.e. at near-threshold levels, can be estimated by means of the following simple model. Consider first an idealized crack, shown in Fig. 18a, where the excess oxide layer is taken to be a rigid wedge of constant thickness d, extending along the crack length a distance 2ℓ behind the crack tip. Assuming only a mechanical closure phenomenon arising from the presence of the excess oxide debris on the crack faces and ignoring plasticity and hysteresis effects, calculations based on elastic superposition using Barenblatt singular integral equations (50) or the Westergaard stress function (51) yield a closure stress intensity value at the crack tip (52)

$$K_{c\ell}\bigg|_{x=0} = \frac{Ed}{4\sqrt{\pi\ell}(1-\nu^2)} , \qquad (3)$$

where d is the maximum excess oxide thickness, 2ℓ the location behind the tip corresponding to the thickest oxide formation and $E/1 - \nu^2$ the effective Young's modulus in plane strain. An estimate of 2ℓ can be obtained from scanning electron microscopy of fatigue specimens, broken open in liquid nitrogen after cycling at threshold ΔK_o levels. From such micrographs, the location of the oxide peak behind the crack tip for SA542-3 steel in air (R = 0.05) was found to be between 1/2 to 5 μm. (It should be noted that because of a square root dependence of ℓ in Eqn. 3, the exact numerical value becomes less critical.) With ℓ = 2 μm, and a maximum oxide thickness of d = 0.2 μm (Fig. 17), an estimate of the closure stress intensity $K_{c\ell}$ is found to be 4.5 MPa$\sqrt{m}$. For tests at R = 0.05 in dry hydrogen, where d = 0.1 μm, $K_{c\ell}$ is estimated to be about 2.3 MPa$\sqrt{m}$. Thus, the predicted difference in closure stress intensities for moist air and dry hydrogen near-threshold conditions, due to the presence of oxide debris, is of order 2 MPa$\sqrt{m}$, approximately equal to the difference in observed threshold ΔK_o values for the two environments
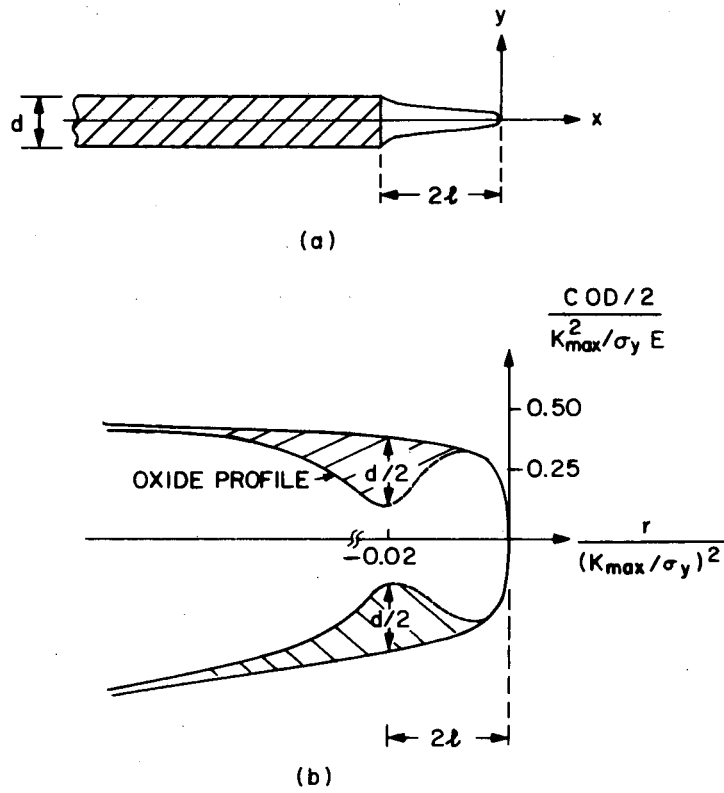
-39-

Figure 18.   Idealizations of oxide wedge inside near-threshold crack.

(Fig. 4). Thus, despite the crude nature of the model and the assumption that the levels of plasticity-induced closure are identical in both environments, it is clear that corrosion deposits formed on crack faces at the thicknesses measured have a significant influence on closure stress intensities at near-threshold levels, where crack tip displacements are small.

A more realistic idealization (53) of the situation is shown in Fig. 18b where the measured oxide profile, for SA542-3 steel in moist air at R = 0.05 (Fig. 17), is superimposed on the crack opening profile (for a solid of strain hardening exponent n' = 0.1), as determined from Shih's small-scale yielding finite element solution, for monotonic loading using J_2 deformation theory (54). By comparing the maximum oxide thickness with the normalized crack opening displacement (COD/$(K_{max}^2/E\sigma_y)$), as a function of normalized distance from the crack tip $(r/(K_{max}/\sigma_y)^2)$, it is again apparent that significant crack closure can arise from the presence of sub-micron corrosion deposits. However, because of uncertainties associated with the location of the maximum oxide thickness behind the crack tip at ΔK_o, with the exact nature of contact between the crack faces, and with the oxide profile from the oxide peak to the crack tip, more rigorous calculations of K_{cl} are not feasible at present.

Approximate calculations for closure levels have also been performed by Purushothaman and Tien (55), where an estimate of the closure stress intensity K_{cl} was derived in terms of the interference between mating fracture surfaces. In their surface roughness model for fatigue crack closure, the influence of fracture surface undulation is considered, such that

$$h = h_o \exp (\varepsilon_f), \qquad (4)$$

where h_o and h are length dimensions describing the initial and final fracture surface roughness, and ε_f the true fracture ductility representative of the stress state ahead of the crack tip. By equating the change in asperity height $\alpha(h-h_o)$, where α is an unknown constant less than unity, to the crack tip opening displacement, estimates of K_{cl} were derived. The model does not, incidentally, incorporate the role of crack tip Mode II displacements characteristic of near-threshold crack growth (48), which will markedly influence the extent of interference (56). However, despite

-41-

this and uncertainties in the empirical CTOD expression and in the constant α, this simple model does yield reasonable estimates of $K_{c\ell}$ (55).

Thus, at the small crack tip opening displacements associated with near-threshold fatigue crack growth, it appears that crack opening or closing loads can be enhanced by the presence of foreign debris.

Comparisons of the maximum excess oxide thickness at threshold, from Auger measurements (Fig. 17), with computed cyclic crack opening displacements (ΔCTOD) for different classes of 2¼ Cr-1Mo pressure vessel steels, derived from Shih's calculations for plane strain (56), reveal that at the threshold stress intensity (ΔK_o) the two parameters are of similar magnitude (Table 4 and Fig. 19). Despite inherent uncertainties in the Auger sputtering measurements and in ΔCTOD computations, this suggests one physically appealing rationale for the existence of a threshold, in that the crack will cease to propagate when it becomes wedged-closed, such that ΔK_{eff} tends to zero. The variation in ΔK_o for wet and dry environments, at different load ratios, and with varying yield strength are consistent with this mechanism. Further, based on this model, one would not expect to find a well-defined threshold for tests _in vacuo_, except perhaps at smaller crack tip displacements where other sources of closure, such as resulting from fracture surface morphology, may play a role. While interpretations of such a result may be masked by rewelding effects, the vacuum data of Cooke et.al. (10) and Skelton and Haigh (12) on medium strength steels do not in fact show a well-defined threshold.

From the above results and discussions, it is clear that in dry environments, such as dehumidified hydrogen or helium (where the availability of moisture is less compared to humid environments), and at high load ratios (where closure due to plasticity is smaller), the formation of excess oxide debris is restricted. In such cases, the closure due to corrosion debris is clearly smaller, the effective stress intensity range value is larger and hence the resulting threshold values are lower compared to humid atmospheres. In other words, near-threshold crack growth rates are accelerated in the presence of hydrogen compared to air, not because of hydrogen embrittlement _per se_, but due to a smaller amount of closure in gaseous hydrogen as opposed to moist air. This is consistent

TABLE 4
Threshold Data for 2¼ Cr-1Mo Steels

Steel	Environment	R	ΔK_o	CTOD[1]		Max. Oxide Thickness
				cyclic	max	
			(MPa√m)	(µm)	(µm)	(µm)
SA542-3	moist air	0.05	7.7	0.18	0.31	0.20
(σ_y = 500 MPa)	moist air	0.75	3.2	0.03	0.78	0.01
	dry H_2	0.05	5.2	0.08	0.14	0.09
	dry H_2	0.75	3.3	0.03	0.83	0.01
	dry He	0.05	6.2	0.11	0.20	0.10
	water	0.05	7.8	0.18	0.32	0.25
SA542-2	moist air	0.05	7.1	0.11	0.17	0.12
(σ_y = 769 MPa)	moist air	0.75	2.8	0.02	0.41	-
	dry H_2	0.05	4.6	0.04	0.07	0.04
	dry H_2	0.75	2.8	0.02	0.38	-
	dry He	0.05	4.9	0.05	0.08	0.04
	dry He	0.75	2.7	0.02	0.35	-
SA542-2/ T690	moist air	0.05	8.6	0.19	0.34	0.16
(σ_y = 575 MPa)	dry H_2	0.05	6.9	0.12	0.22	0.11
	dry He	0.05	7.1	0.13	0.23	0.11

[1] Plane strain values defined as 0.50 ($\Delta K_o^2/2\sigma_y'E$) - cyclic, and 0.50 ($K_{max,o}^2/\sigma_y E$) - maximum, where ΔK_o and $K_{max,o}$ are the cyclic and maximum threshold stress intensities, σ_y' and σ_y are the cyclic and monotonic yield strengths, and E is the elastic modulus.
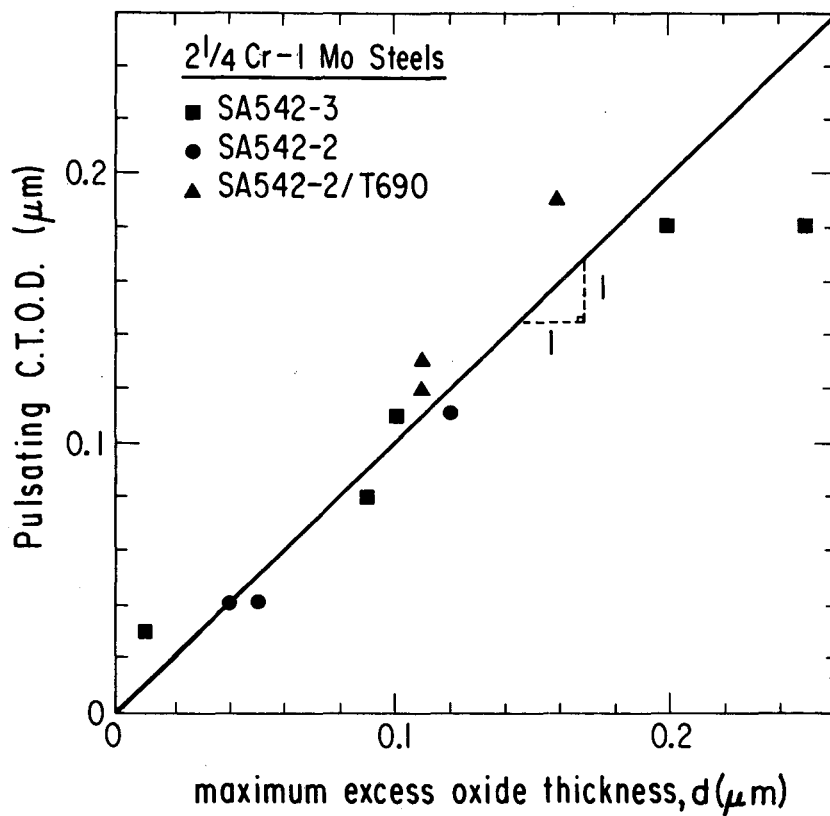
Figure 19. Correlation between oxide thickness and cyclic CTOD at ΔK_o.

with the oxide thickness measurements, the observation that hydrogen influences threshold behavior only at low load ratios and the fact that there is no change in characteristic fracture mode.

The influences of load ratio and strength on the threshold values also follow from such closure concepts (42). The variation of the measured threshold ΔK_o values in both moist air and hydrogen environments is shown in Fig. 20. At low load ratios, threshold values are apparently greater compared to those at higher load ratios because of the effect of plasticity-induced crack closure. In moist environments, this closure is further enhanced by oxide-induced crack closure compared to dry environments. However, above a critical R value (about 0.58 for SA542-3 steel), both these closure modes are minimized and there is no influence of load ratio or environment. The nomenclature for threshold stress intensity parameters and their variation with load ratio are shown in Fig. 21 (47). It is assumed that a minimum positive stress intensity, $K_{c\ell}$, is necessary to open a crack and that the effective threshold stress intensity range, $\Delta K_{eff} (= K_{max} - K_{c\ell})$, necessary to propagate a fatigue crack is roughly constant. At low load ratios ($K_{min} < K_{c\ell}$), where the measured threshold values ΔK_o are apparently higher than those for higher load ratios because of plasticity-induced closure in dry environments and both plasticity-induced closure and oxide-induced closure in moist environments, it is seen that the maximum stress intensity value corresponding to threshold ΔK_o is a constant, i.e. $K_{o,max} = K_{c\ell} + \Delta K_{eff}$. However, at high load ratios, where the minimum stress intensity K_{min} is greater than $K_{c\ell}$, there is little effect of closure and hence the measured and the actual threshold alternating stress intensity values are approximately the same. The value of R at which the minimum stress intensity becomes equal to $K_{c\ell}$, i.e. $R_{c\ell}$, is the critical load ratio corresponding to the transition from a constant $K_{o,max}$ behavior to a constant ΔK_o, R-independent behavior. It is important to note from Fig. 20 that $R_{c\ell}$ corresponding to moist air and hydrogen environments is about 0.6 and 0.3, respectively. The fact that this critical load ratio is higher in moist air than in hydrogen is indicative of higher closure loads due to enhanced oxide debris formation.

Finally, the reduction in threshold ΔK_o values with increasing material strength and the fact that the effect of hydrogen in ultra-high strength steels is apparently smaller (1) may also be consistent with
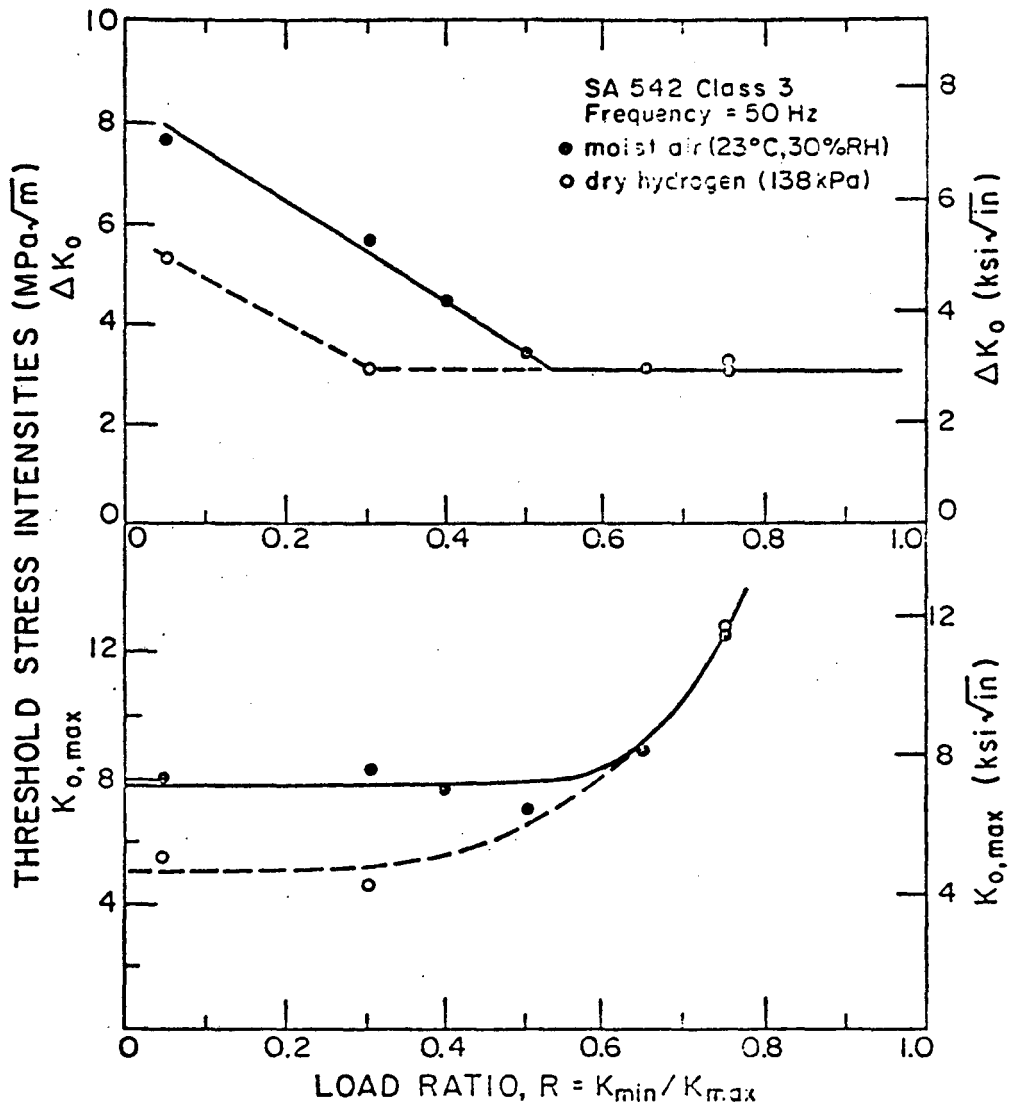
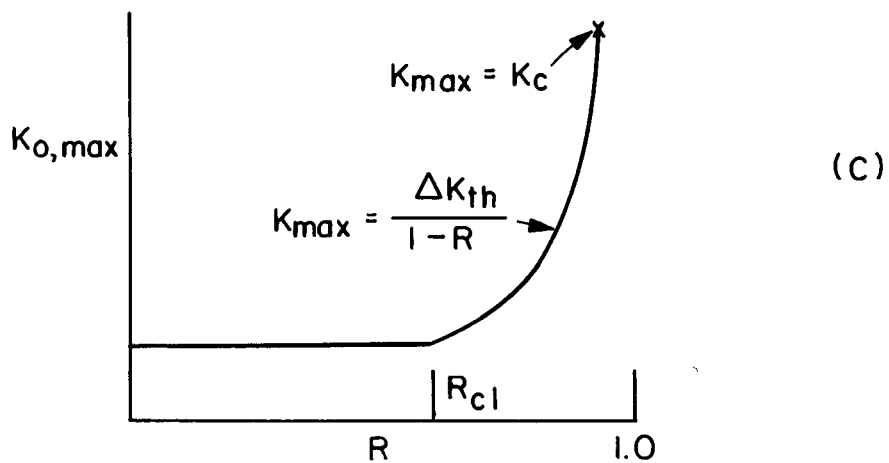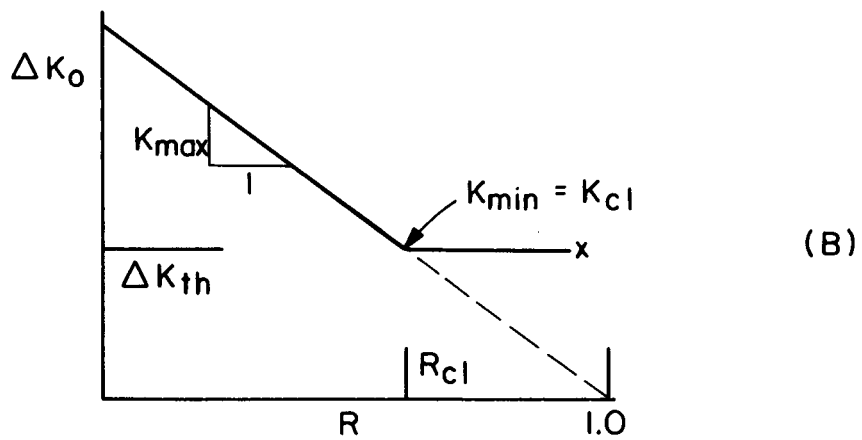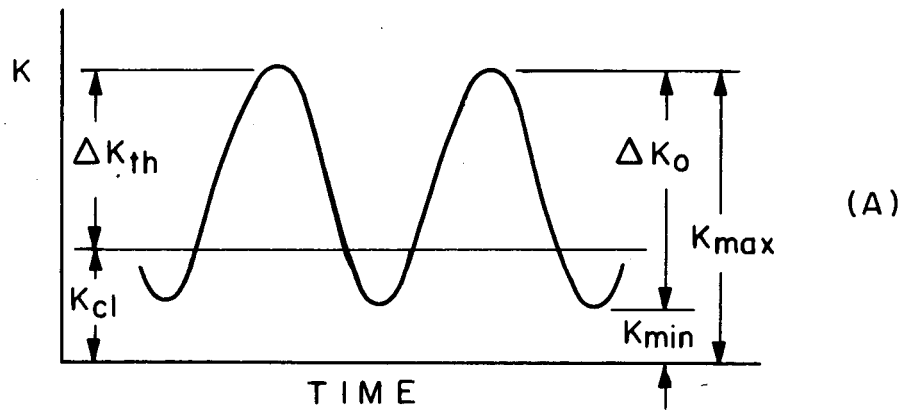Figure 20. Variation of threshold stress intensity parameters with load ratio.

Figure 21. Nomenclature for stress intensity parameters at threshold and their variation with load ratio R (after Schmidt and Paris (47)).

this model, since plasticity-induced crack closure would be expected to be reduced in higher strength materials and further, fretting damage from oxide debris would be somewhat less severe on the harder fracture surface of a high strength material.

Results of a number of studies in the literature show evidence supporting the oxide-induced crack closure model. Such data, along with measurement of closure using ultrasonic techniques are discussed in the following section.

5. OXIDE-INDUCED CRACK CLOSURE: SUPPORTING EVIDENCE

5.1 Introduction

Evidence in support of the concepts of oxide-induced crack closure can be readily found in the literature. The idea of corrosion deposits forming in cracks and influencing subsequent growth behavior is not entirely new. For example, threshold results for pressure vessel and rotor steel have been found to show somewhat higher ΔK_o values in water than in air (6, 44). Tu and Seth (9) report slower near-threshold growth rates in several rotor steels tested in 100°C in the seemingly more aggressive environment of steam compared to air; a fact they attribute to a number of factors including crack tip corrosion deposits. In fact, observation of corrosion debris has traditionally provided a means to detect and monitor the growth of incipient flaws under service conditions in many aircraft components (60). Studies by Swanson and Marcus (61) as well as Benoit et.al. (49) clearly show that the phenomenon of enlarged oxide formation is a result of the fatigue process itself and that the amount of oxide diffusion into the material in the presence of moist environments during fatigue crack growth is far greater than that in the same environment in the absence of crack growth. Results of Mahulikar and Marcus (62) reveal that in humid environments, residual displacements on the faces of fatigue specimens are higher compared to those in vacuum due to the build up of oxides on fracture faces. Fatigue data by Nordmark and Fricke (63) explain crack arrest during fatigue of 7475 aluminum alloys in sump water using arguments of crack tip corrosion deposits. Skelton and Haigh (12) interpret their results of lowered ΔK_o values in vacuo and at R = -1 in Cr-Mo-V steels at 550°C in terms of reduced crack tip opening displacements from shear lips and oxide-filling of the crack. It has become clear that several hitherto unexplained experimental observations cited in the literature can be understood in terms of the concepts of crack closure induced by corrosion deposits.

The results on environmental effects in the near-threshold region of crack propagation (presented in the previous chapter) clearly support the concepts of oxide-induced crack closure. The fact that, with reference to moist air, near-threshold growth rates are accelerated in dry hydrogen

and dry helium and marginally decelerated in distilled water while
showing the same behavior in wet hydrogen must be considered as some-
what confusing when viewed in the light of conventional corrosion
fatigue mechanisms. However, these results clearly demonstrate that
the significant role of environment near-threshold at low load ratios
depends principally on the availability of moisture rather than on the
embrittling tendency of any specific environmental species. This
behavior is clearly follows from the result that while dry hydrogen
accelerates near-threshold crack growth rates by up to 20 times, wet
hydrogen leads to a threshold behavior similar to moist air. Recent
data (64) on SA387, Class 2, Grade 22 steel have shown that moisture
(and not oxygen) is responsible for thick oxide formation. In this
material, near-threshold growth rates in dry oxygen are found to be
similar to those in dry air and dry hydrogen and are significantly
higher than those in moist air.

5.2 Direct Measurement of Closure Using Ultrasonics

To provide direct experimental evidence of the phenomenon of oxide-
induced crack closure, actual closure measurements were performed as
near-threshold cracks using an ultrasonic technique. The procedures were
performed using the equipment of Williams and DeLonga (65) based on
techniques developed initially by Frandsen et.al. (66).

A series of compact tension specimens were prepared containing 26 mm
cracks grown to the threshold stress intensity in moist air at R = 0.05
and 0.50 and in dry hydrogen at 0.05. Ultrasonic waves, with a frequency
of 2 MHz, were transmitted at one edge of the specimen and were received
at the opposite end as shown schematically in Fig. 22, while the specimen
was mounted on the testing machine for application of the load. The
specimen was subjected to loads corresponding to stress intensity values
ranging from zero to about 8.5 MPa$\sqrt{m}$ (slightly above the K_{max} values
corresponding to the threshold ΔK_O of 7.7 MPa$\sqrt{m}$ at R = 0.05). The
amplitude of the signal transmitted to the specimen was kept a constant
and the transmitted output from the receiver was monitored with an
oscilloscope. There was no variation in the receiver signal up to a
certain load level beyond which there was a decrease in the signal
amplitude. This is due to the fact that as the crack starts to open, a
lesser amount of the signal is transmitted to the receiver leading
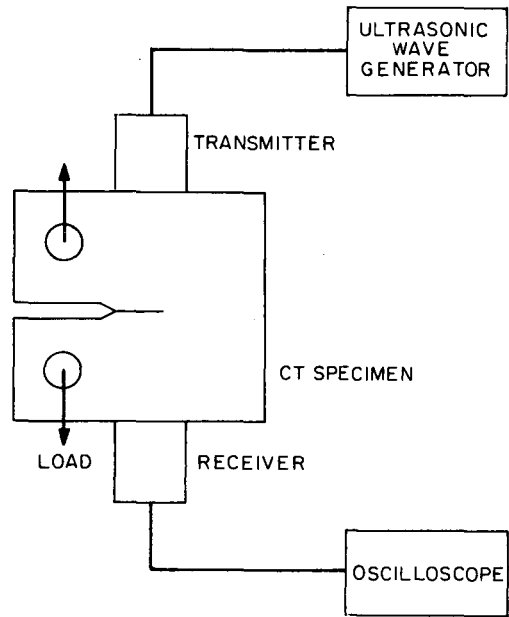to a reduction in the signal amplitude. After a gradual decrease,

Figure 22.   Schematic showing the location of transducers on the compact tension specimen for ultrasonic testing.

receiver signal amplitude again reached a constant value. The loads
were then dropped to the zero level to check for repeatability. There
was no noticeable difference between the receiver signals for increasing
and decreasing loads.

The variation of receiver output signal is plotted against the
stress intensity factor for closure tests conducted on specimens fatigue
cracked to threshold ΔK_o values in both air and hydrogen atmospheres
(Fig. 23). It is seen that there is no steep decrease in the receiver
output implying that the crack does not open all at once, but does so
rather gradually. This is in agreement with the observation of
Bachmann and Munz (67) that crack surfaces can remain in contact locally,
while globally the crack can be considered fully open. Although no
precise estimation for the crack closure stress intensities, $K_{c\ell}$, could
be obtained, it is observed that the stress intensity levels at which
the receiver output signal value decreases is of the order of the
closure K values (roughly equal to K levels at threshold in air and
hydrogen). The most important observation of these tests is that crack
opening occurs at a higher stress intensity value for the specimen
tested in moist air compared to that tested in hydrogen, confirming the
occurrence of increased crack closure near-threshold due to oxide
deposits.

To check the validity of the closure tests, two additional experi-
ments were conducted. When a specimen with no fatigue crack was tested,
there was no variation in the receiver signal while the applied loads
were increased from zero to threshold levels (Fig. 24), and this constant
output was the same as that obtained with no load on the specimens thres-
hold-tested in air and hydrogen. Also, a specimen with a saw cut equal
in length to the crack length of the fatigue-cracked specimens showed no
change in the receiver output with increasing loads. However, the
amplitude of the output signal for the case of the saw cut specimen was
much smaller than the initial output amplitudes of the uncracked and
the precracked specimens.

The tests conducted using ultrasonic waves indicate that the
closure loads for threshold tests in moist air are higher than those in
dry hydrogen. As a result of the uncertainties involved in using this
technique and in view of the fact that the crack surfaces may be in
contact locally (similar to the growing region of Hertzian contact) while
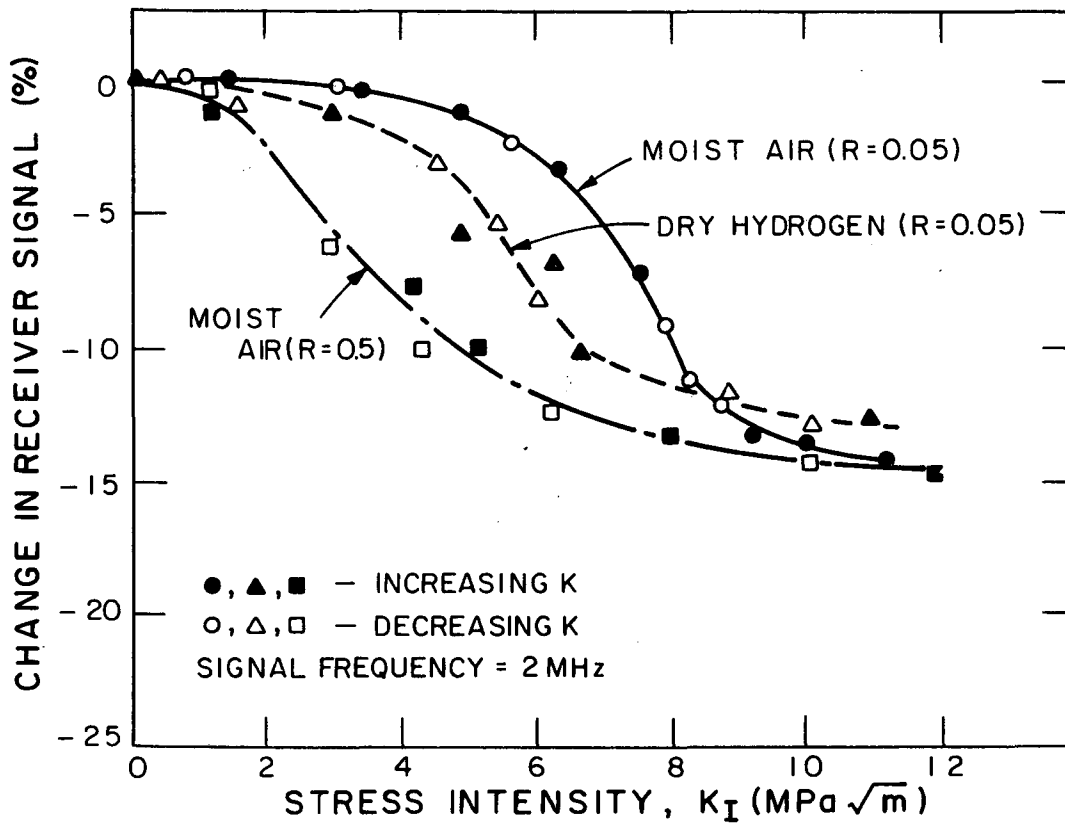
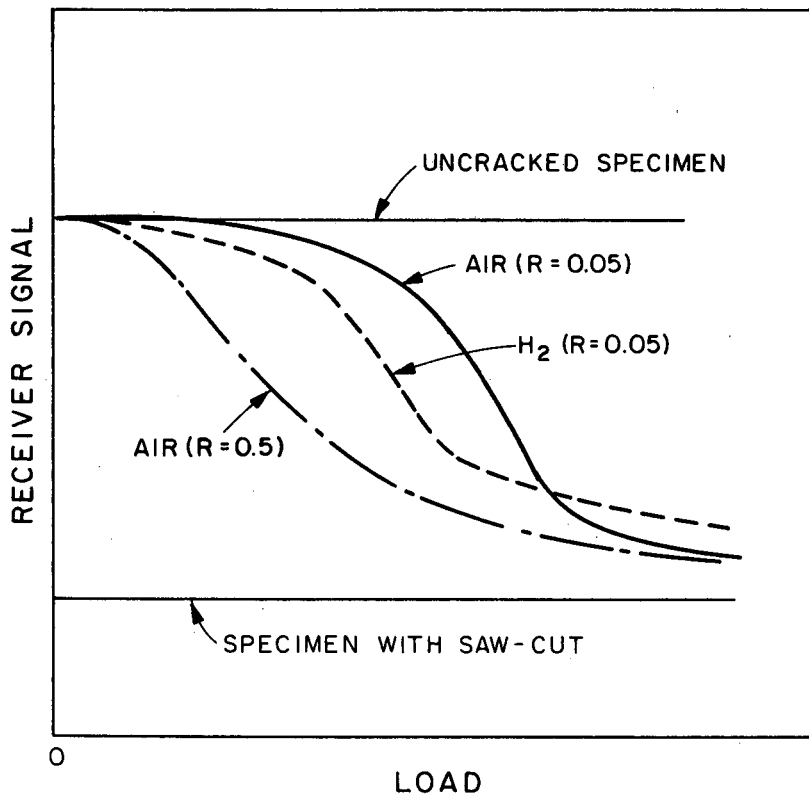Figure 23.   Variation of receiver signal with stress intensity.

Figure 24.   Schematic showing receiver signal output for uncracked, saw-cut and fatigue-cracked specimens.

macroscopically the crack may remain closed, a single closure load
cannot be meaningfully estimated.

6. INFLUENCE OF FATIGUE UNDERLOADS (SUB-THRESHOLD)

Transients in growth rate behavior induced by single overloads or various spectrum loading sequences have been attributed to such mechanisms as residual compressive stresses (68, 69), cyclic strain hardening (70), crack tip blunting (71), and plasticity-induced closure (45). Since such phenomena are common to airframe components many of these studies have been performed with thin sheets (68, 69, 72-74), under essentially plane stress conditions, where mechanisms such as plasticity-induced crack closure can be predominant (45).

In this work, however, the role of variable amplitude loading under fully plane strain conditions is examined. Specifically, the influence of block cycling below the threshold stress intensity for no crack growth (ΔK_o) is considered (1). Such underloads may occur within certain loading spectra, and in the laboratory during standard load shedding procedures (1, 75) for measuring near-threshold growth rates at low stress intensities. For example, since measurement of such near-threshold crack growth at conventional frequencies can be so time consuming, it is often necessary to interrupt the test, by say stopping or "parking" overnight at a ΔK level below the threshold ΔK_o where presumably no damage can occur. Where such interruptions have been reported (76), unexplained transients in crack growth behavior often result and behavior after the interruption is initially very different from behavior before, for nominally identical conditions. In the present work, the influence of periodic cycling at ΔK levels below the threshold ΔK_o is examined on near-threshold fatigue crack propagation in SA542-3. The transient growth rate behavior is rationalized in terms of oxide-induced crack closure.

The influence of variable maplitude loading was examined under constant ΔK cycling (R = 0.05) using load sequences illustrated in Fig. 25. After load shedding to near-threshold levels, cracks were grown for 1-1.5 mm at a constant baseline ΔK level (ΔK_B), whereupon a sub-threshold underload ΔK level (ΔK_U) was applied for 2.7 x 10^6 cycles (15 hrs at 50 Hz), before conditions were returned to the original ΔK_B baseline level. A series of tests were performed for baseline levels of ΔK_B = 8.3 - 10 MPa$\sqrt{m}$, with underloads (below ΔK_o) of ΔK_U = 4 - 7.5 MPa$\sqrt{m}$. From crack length (a) versus number of cycles (N) data monitored during the sequence, the following

-56-

parameters were defined (Fig. 25), namely $(da/dN)_B$ the baseline crack growth rate at ΔK_B, $(da/dN)_S$ the initial crack growth rate at ΔK_B following the underload period, and a^* and N^* representing the crack length and number of cycles at ΔK_B following the underload period before growth rates returned to their original baseline value $(da/dN)_B$.

Effects of sub-threshold underloads $(\Delta K_U < \Delta K_O)$ on near-threshold crack growth rates at baseline ΔK_B levels between 8.3 and 10 MPa√m (R = 0.05) are shown in Fig. 26. Data pertinent to this figure in terms of parameters defined in Fig. 26 are listed in Table 5. Although no crack growth was ever detected during the 2.7×10^6 underload cycles, subsequent crack growth was in certain cases severely affected. Little effect was apparent after an underload of $\Delta K_U = 4$ MPa√m on baseline growth rates at $\Delta K_B = 10$ MPa√m (Fig. 26a). Similarly, underload cycling at $\Delta K_U = 6.5$ MPa√m had only a small influence on crack growth at $\Delta K_U = 9$ MPa√m (Fig. 26b). Application of cyclic underloads fractionally below the threshold at $\Delta K_U = 7.5$ MPa√m, however, resulted in significant decelerations in subsequent baseline growth rates at ΔK_B between 8.3 and 10 MPa√m (Fig. 26c-f). Following the underload periods, initial growth rates were up to 5 times slower than pre-underload baseline rates, with retardations experienced over crack growth increments a^* up to 0.3 mm (equivalent to several times the maximum plastic zone sizes at ΔK_B).

Thus periods of underload cycles beneath the threshold ΔK_O, where presumably no crack growth damage can occur, can give rise to transient retardations in near-threshold crack growth rates over distances comparable with several maximum plastic zone sizes, the magnitude of the retardation depending both on the baseline and underload stress intensity ranges applied.

It has been shown that, in certain circumstances, cycling below the threshold stress intensity ΔK_O can retard subsequent near-threshold crack growth rates, a phenomenon somewhat analogous to the well known effect of "coaxing" where smooth specimens cycled below the fatigue limit are often found to possess improved resistance to fatigue failure. However, whereas coaxing has been attributed to strain againg effects (77), a mechanism for the influence of sub-threshold underloads is peresented below in terms of oxide-induced crack closure arguments.

It has been shown in previous sections that oxide thicknesses increase with decreasing growth rates and hence with decreasing ΔK levels as the threshold is approached. Furthermore, from oxide thickness measurements it
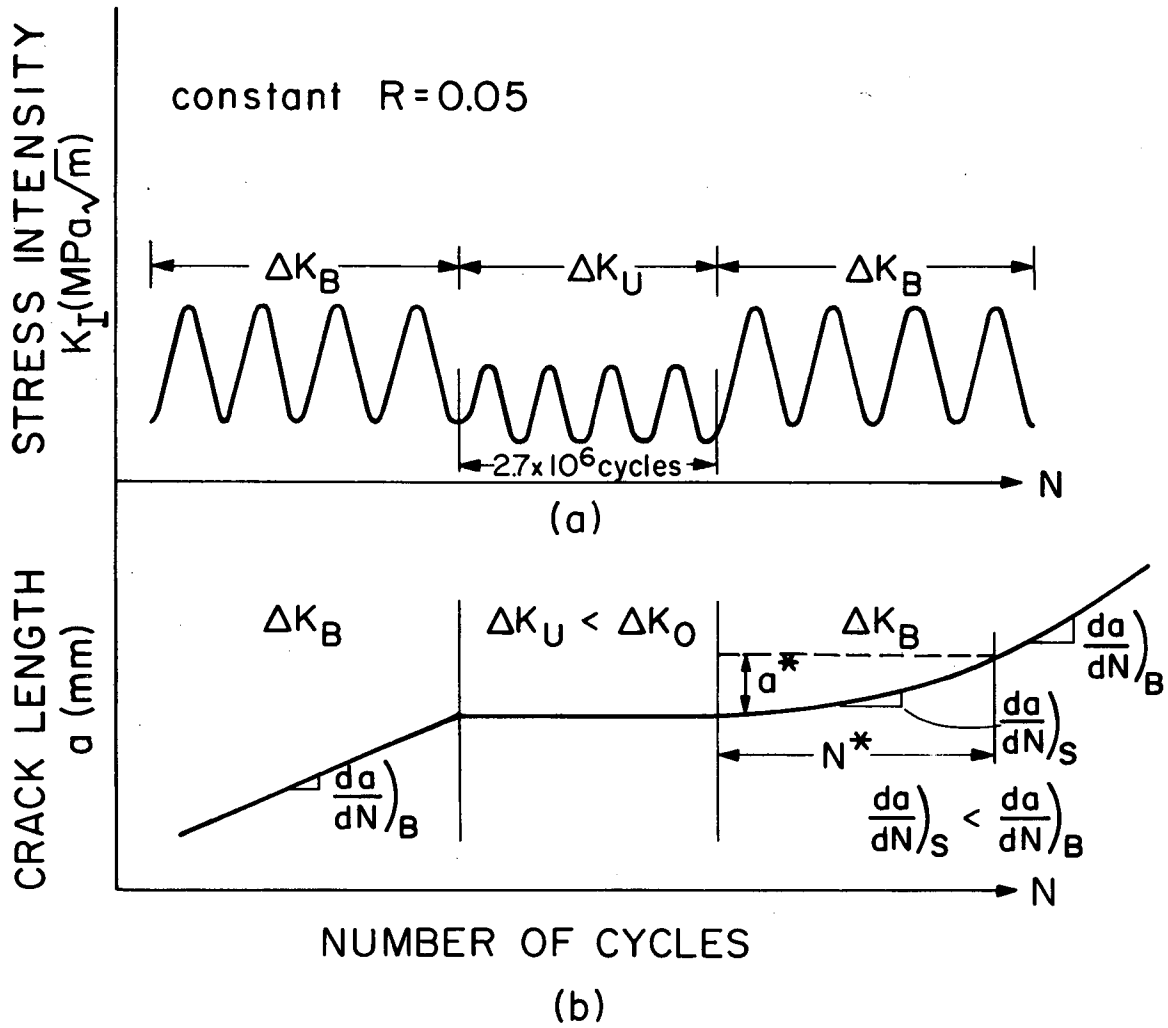
-57-

Figure 25. Nomenclature of different parameters used to describe the underload interactions near threshold.
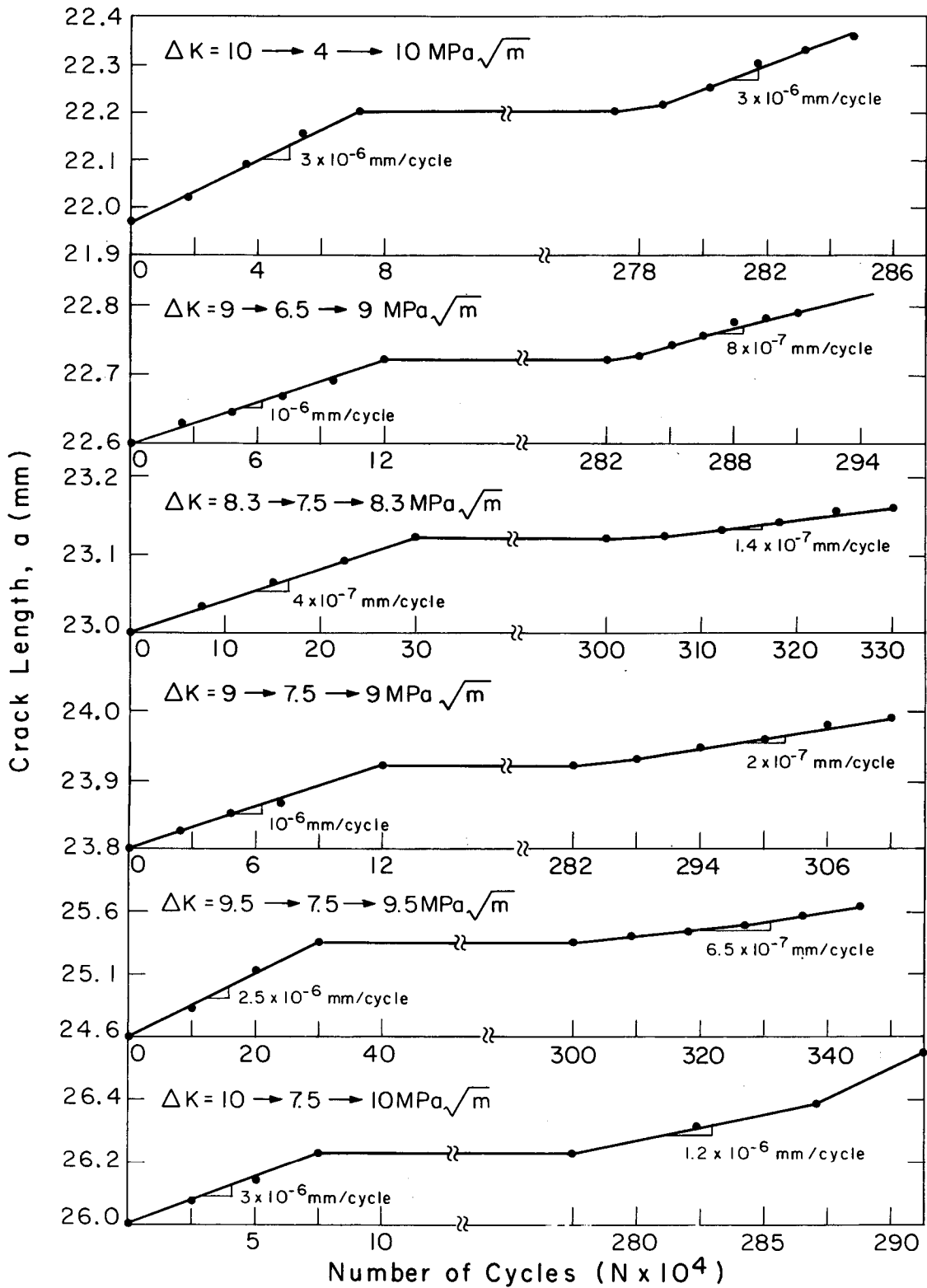
Figure 26. Crack length versus the number of cycles showing the effects of underloads.

TABLE 5

Results of Variable Amplitude Tests Involving Effect of Underloads (ΔK_U) on Near-Threshold Growth

Test No.	$\Delta K_B \rightarrow \Delta K_U \rightarrow \Delta K_B$ (MPa$\sqrt{m}$)	$\frac{da}{dN}_B \rightarrow \frac{da}{dN}_S$ (mm/cycle)	a* (mm)	N*, (no. of cycles)
a	$10 \rightarrow 4 \rightarrow 10$	$3 \times 10^{-6} \rightarrow 3 \times 10^{-6}$	0.010	1.5×10^4
b	$9 \rightarrow 6.5 \rightarrow 9$	$1 \times 10^{-6} \rightarrow 8.5 \times 10^{-7}$	0.008	1.5×10^4
c	$8.3 \rightarrow 7.5 \rightarrow 8.3$	$4 \times 10^{-7} \rightarrow 1.4 \times 10^{-7}$	0.100	8.0×10^5
d	$9 \rightarrow 7.5 \rightarrow 9$	$1 \times 10^{-6} \rightarrow 2 \times 10^{-7}$	0.140	6.5×10^5
e	$9.5 \rightarrow 7.5 \rightarrow 9.5$	$2.5 \times 10^{-6} \rightarrow 6.5 \times 10^{-7}$	0.300	5.0×10^5
f	$10 \rightarrow 7.5 \rightarrow 10$	$3 \times 10^{-6} \rightarrow 1.2 \times 10^{-6}$	0.240	1.5×10^5

was inferred that cracks would not propagate when the maximum excess oxide thickness equals the pulsating crack tip opening displacement (ΔCTOD). Thus, for particular combinations of baseline ΔK_B and underload ΔK_U, it follows that if the excess oxide thickness d formed at baseline ΔK_B is less than the ΔCTOD at underload ΔK_U, then the application of sub-threshold underload cycles, while not generating fatigue damage per se, can result in further oxide formation due to fretting oxidation mechanisms. Thus, on returning to the baseline ΔK_B level following the underload cycling, one might expect in this instance some initial retardation in crack growth rates due to the increased crack closure loads from the extra oxide deposits formed at ΔK_U. If, on the other hand, the excess oxide thickness d at ΔK_B is already larger than the underload ΔCTOD, then little effect of the underload cycling would be expected since during the latter period the crack would be effectively wedged-closed thereby limiting further oxidation.

This concept is illustrated in Fig. 27, where the variation of crack growth rates (da/dN), experimentally measured oxide thickness (d) and computed underload pulsating crack tip cyclic CTOD values are plotted. Considering first the situation of a baseline ΔK_B for 10 MPa$\sqrt{m}$, the oxide thickness generated at this level has been measured to be approximately 0.11 μm (Fig. 27). When an underload of ΔK_u = 4 MPa$\sqrt{m}$ is applied, the corresponding ΔCTOD is roughly 0.05 μm, smaller than the existing oxide thickness, such that the crack remains closed. With no enhancement in oxide-induced crack closure, therefore, an underload of 4 MPa$\sqrt{m}$ would be expected to have little effect on growth rates at 10 MPa$\sqrt{m}$, in accordance with experimental observations (Fig. 26a and Table 5). Conversely, when an underload of ΔK_U = 7.5 MPa$\sqrt{m}$ is applied at ΔK_B = 10 MPa$\sqrt{m}$, the underload ΔCTOD is now roughly 0.17 μm, larger than the existing (baseline) oxide thickness, such that some further oxide growth can occur. With the resulting enhancement in oxide-induced crack closure, the 7.5 MPa$\sqrt{m}$ underload would be expected to cause some initial retardation in growth rates at ΔK_B = 10 MPa$\sqrt{m}$ consistent with experimental results (Fig. 26f and Table 5). Similar arguments are applicable to the other results in Fig. 26.

It also follows from this discussion that at each baseline ΔK_B level, a critical underload stress intensity range (ΔK_{UC}) would exist below which underloads can have little effect. This corresponds to an underload ΔK_U level below which the crack remains closed, i.e. where the underload ΔCTOD
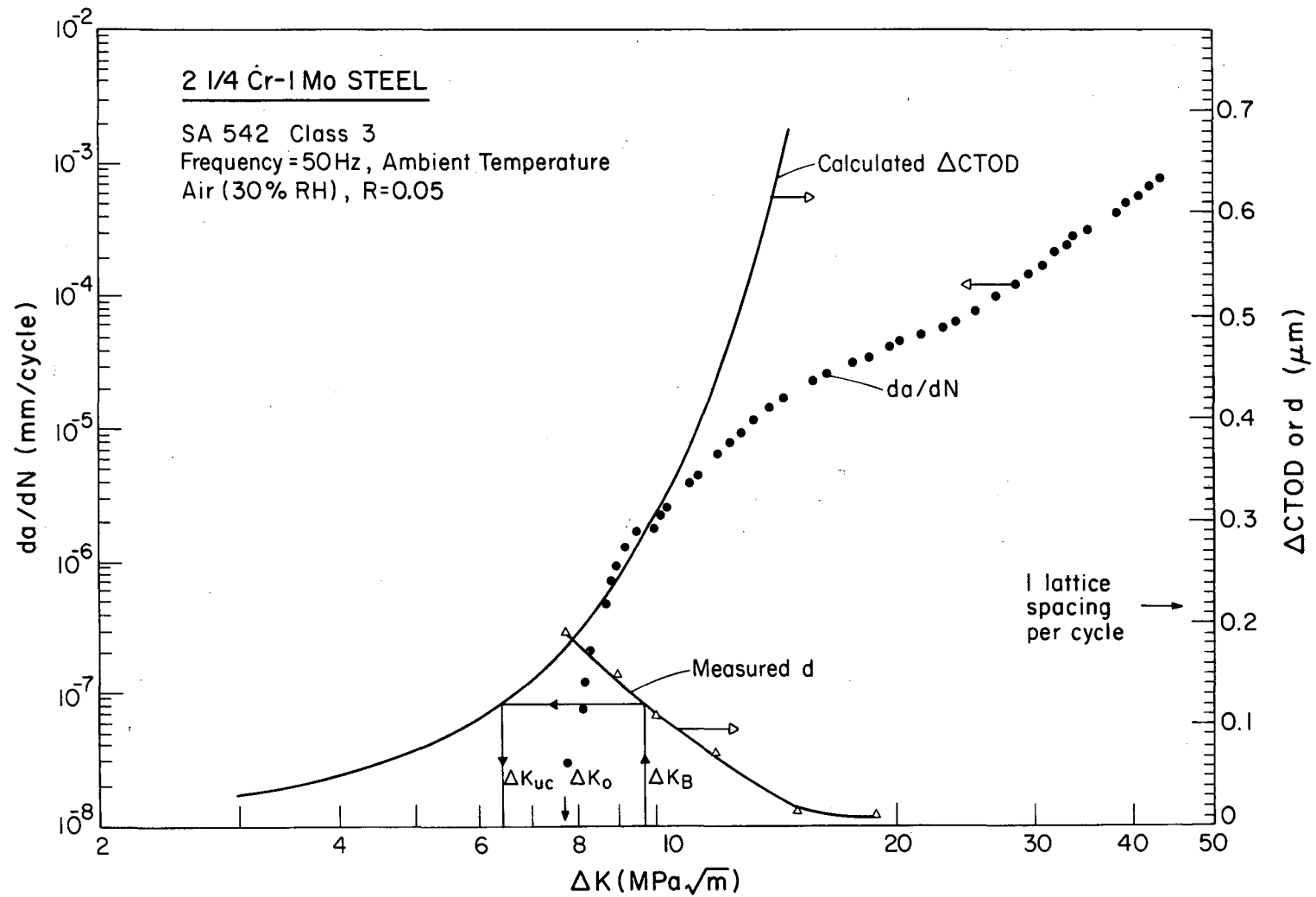
Figure 27. Variation of cyclic CTOD, oxide thickness d, and crack growth rate with stress intensity range and a scheme for finding the critical underload stress intensity range.

is less than the existing oxide thickness (d). For crack growth at ΔK_B = 10 MPa$\sqrt{m}$ (where d = 0.11 μm), this corresponds to an underload level of ΔK_U = 6 MPa$\sqrt{m}$. Hence underloads at 7.5 MPa$\sqrt{m}$ can lead to subsequent retardations whereas underloads at 4 MPa$\sqrt{m}$ have little effect (Table 5). Similarly, for crack growth at ΔK_B = 9 MPa$\sqrt{m}$ where critical underload level becomes ΔK_U = 7.1 MPa$\sqrt{m}$, underloads at 7.5 MPa$\sqrt{m}$ are seen to reduce growth rates initially by roughly five times, whereas negligible effects are apparent following underloads at 6.5 MPa$\sqrt{m}$ (Fig. 26b and 26d). Using Fig. 27, values of ΔK_{UC} can be estimated graphically for any baseline ΔK_B level, by simply following the direction of arrows in equating oxide thickness (d) at ΔK_B to ΔCTOD at ΔK_U. However, recognizing that oxide-induced crack closure is important only at low stress intensities where crack tip displacements and corrosion deposits are of the same size scale, it is apparent that sub-threshold underloads are only likely to have an effect on near-threshold growth rates. With increasing K levels, the corresponding ΔCTOD increases so rapidly (proportional to ΔK^2) that further oxidation during the underload would be negligible in comparison.

Thus, in summary, it has been shown that near-threshold fatigue crack growth can suffer transient retardations following underload cycling (at the same load ratio) below the threshold. Such crack growth retardations are reasoned to result from enhanced oxide-induced crack closure generated during the underload, provided that the underload ΔCTOD is large enough to allow further oxide growth. The close numerical correspondence between ΔCTOD and crack flank oxide thickness data, however, could be considered somewhat remarkable in view of the uncertainty in the two estimates. However, conceptually such data are totally consistent with an explanation of the experimental observations in terms of oxide-induced crack closure.

In terms of recommended procedures for measuring near-threshold fatigue crack growth and threshold ΔK_0 values (75), such closure concepts could have important consequences. Current practices for threshold determination utilize crack growth monitoring under decreasing ΔK (load-shedding) and/or increasing ΔK conditions, thus, continuously involving variable amplitude loading. Care is generally taken to avoid too rapid a descent in K to mini- mize crack growth retardation and hence premature threshold determination resulting from plasticity considerations. It is now apparent that a further factor may be important in that interrupting tests, by "parking" overnight at ΔK levels below the threshold, may yield similar premature retardations.

Moreover, where oxide-induced closure is significant, one might expect that near-threshold growth rates determined under decreasing ΔK conditions may be somewhat different from those determined under increasing ΔK. In this regard, it is perhaps, significant that materials which are very susceptible to aqueous stress corrosion cracking are often likely to show this behavior (75, 78), possibly reflecting a differing contribution from oxide-induced crack closure arising from the presence of substantial crack flank corrosion deposits.

7. ENVIRONMENTAL EFFECTS IN ULTRAHIGH STRENGTH STEELS

To contrast with role of environment in influencing near-threshold corrosion fatigue crack growth behavior in lower strength steels, a series of similar experiments were performed on 300-M ultrahigh strength steels, tempered to two strength levels.

The variation of fatigue crack propagation rates (da/dN) as a function of the alternating stress intensity (ΔK) at R = 0.05 for the higher strength T300 microstructure is shown in Fig. 28 for environments of moist air and dry hydrogen. The data plotted represent mean values from several individual tests. As observed for lower strength steels, two distinct regimes appear to exist where crack growth behavior is influenced by hydrogen, namely above $\sim 10^{-5}$ mm/cycle and at near-threshold levels. Above 10^{-5} mm/ cycle, although, growth rates in air and hydrogen are similar at 50 Hz, lowering the frequency to 5 Hz results in significantly faster growth rates in hydrogen. This behavior, which has been widely reported by others (27-29), has been attributed to hydrogen embrittlement mechanisms, consistent with an increase in intergranular fracture observed for hydrogen-assisted failures. What is intriguing, however, is the observation that at growth rates below 10^{-6} mm/cycle at 50 Hz frequency, the presence of hydrogen gas actually results in a <u>deceleration</u> in near-threshold propagation rates and a 16% higher threshold ΔK_o value compared to air. Similar behavior is seen in the lower strength T650 microstructure where, at both high and low load ratios (R = 0.05 and 0.70) at 50 Hz, growth rates in air and hydrogen are similar until near-threshold levels, whereupon they become slower in hydrogen (Fig. 29). Threshold ΔK_o values in hydrogen are again between 11 to 15% higher than in air. Since the decelerating influence of hydrogen is both small and surprising, the validity of the data in Fig. 2 was checked by performing a constant ΔK test near the threshold. A crack was grown in hydrogen gas, after load-shedding to just above ΔK at ΔK = 9.3 MPa$\sqrt{m}$, whereupon the environmental chamber was evacuated and flushed with air. The resulting twofold increase in near-threshold growth rates when air was introduced provides an indication that decelerating effect of hydrogen is real (Fig. 30). Fractographically, little difference was apparent between near-threshold cracks grown in either environment: characteristic flat, featureless transgranular fracture surfaces were observed with isolated intergranular facets.
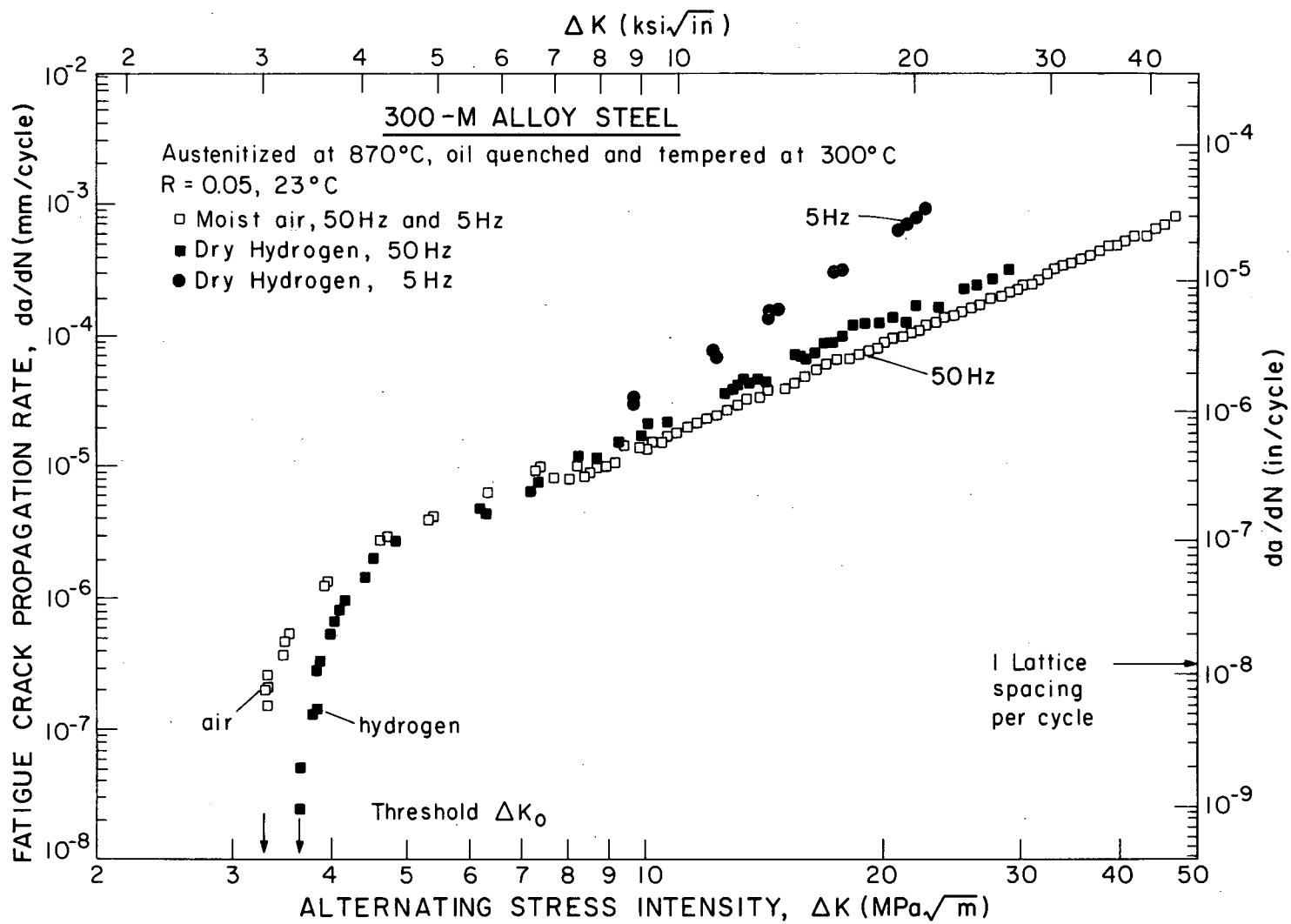
-65-

Figure 28.   Effect of moist air and dry hydrogen on fatigue crack growth
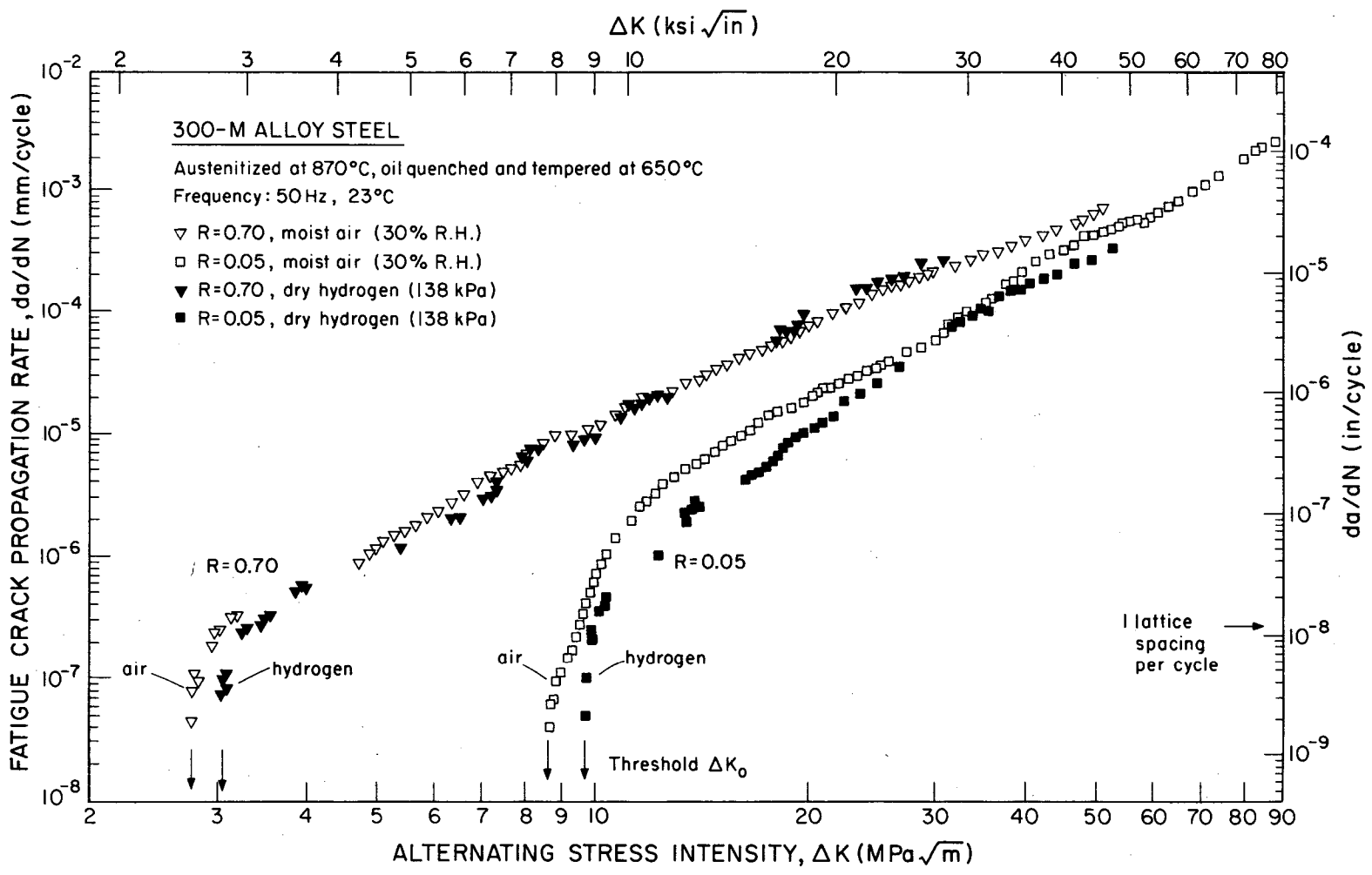in 300°C temper at 5 and 50 Hz (R = 0.05).

Figure 29. Effect of moist air and dry hydrogen on fatigue crack growth in 650°C temper at R = 0.05 and 0.70 (50 Hz).

CRACK LENGTH (mm)

28.0

HYDROGEN | AIR

27.5

da/dN   2.3 10^{-7} mm/cycle

27.0

da/dN 10^{-7} mm/cycle

300M Alloy Steel

Austenitized at 870°C, oil quenched
and tempered at 650°C

26.5

Constant Stress Intensity Test
$\Delta K = 9.3$ MPa$\sqrt{m}$

Frequency : 50 Hz   R = 0.05

26.0

0   36   72   108   144   162   198   234   270   306   342   378
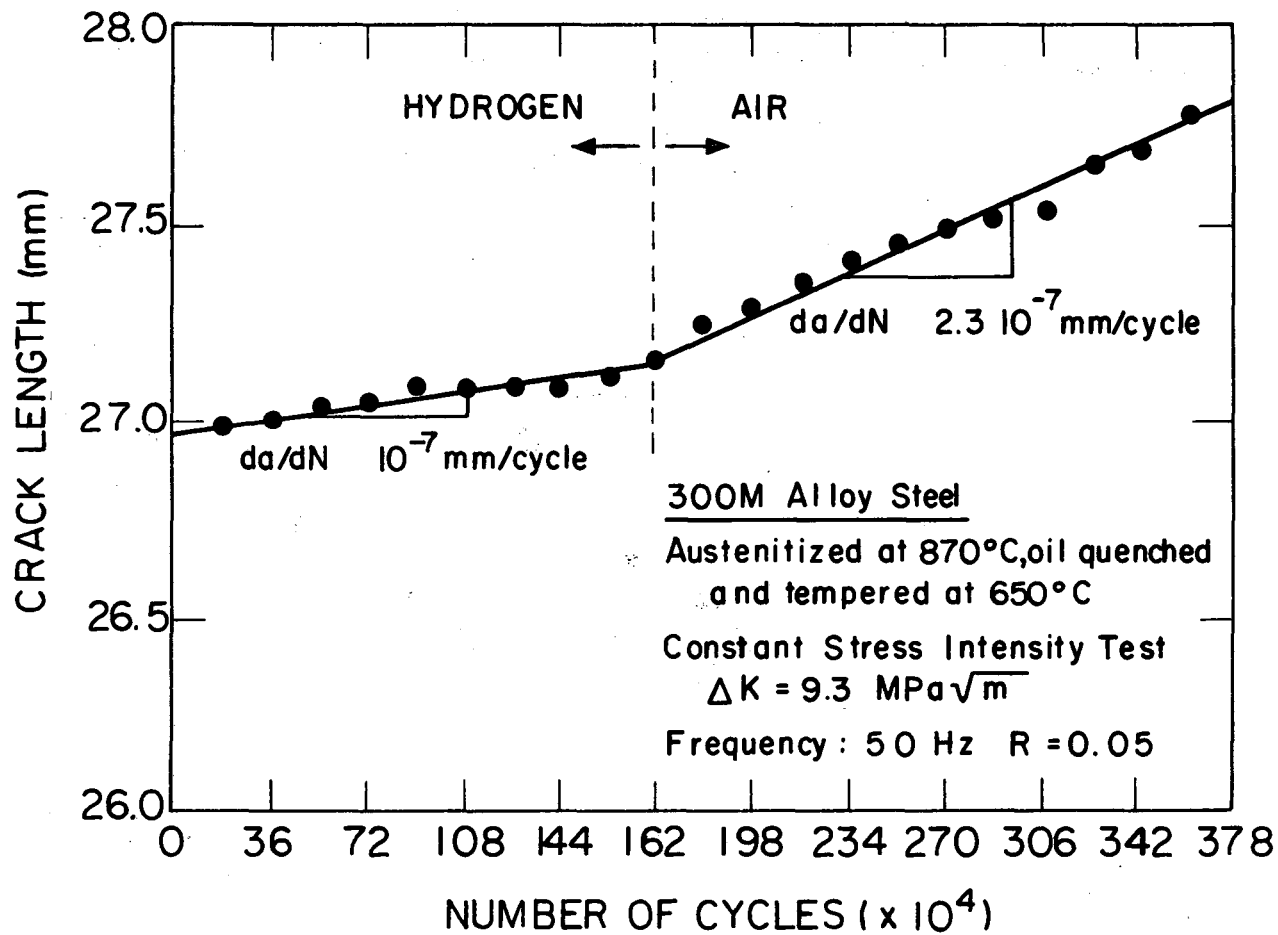
NUMBER OF CYCLES ($\times 10^4$)

Figure 30. Showing two-fold acceleration in near-threshold growth rates in
300-M, tempered at 650°C, on changing environment from dry hydrogen
to moist air. Test performed at constant ΔK = 9.3 MPa$\sqrt{m}$ (R = 0.05)
at 50 Hz.

Similar effects have been recently observed in high strength NiCrMoV rotor steels tested in air and hydrogen (80), although earlier data on a similar material (where no growth rates were measured) showed threshold ΔK_o values to be identical for both environments (43).

Such observations appear to be at variance with conventional mechanisms of corrosion fatigue crack growth, involving hydrogen embrittlement or active path corrosion models (2, 27), and are more surprising in view of the well-known susceptibility of high strength steels such as 300-M to embrittlement from hydrogen, particularly when tempered to peak strength conditions (i.e. at 300°C). Futher, unlike behavior in lower strength steels (42, 44), the observations are also inconsistent with fretting oxide-induced crack closure mechanisms for near-threshold corrosion fatigue (42-44), since closure would only be significant at low load ratios, and lower effective stress intensities would be expected for the moist air environment where presumably oxide formation and hence crack closure would be enhanced. However, the role of such corrosion debris in high strength materials is still unclear at this time since oxide thicknesses are considerably less than in low strength steels. This apparently follows from reduced fretting-oxidation effects arising from less plasticity-induced closure and less abrasion of the oxide debris on the harder steel substrate, and from the fact that the extent of oxide build-up is limited by the smaller crack tip opening displacements (44). Auger measurements of oxide thicknesses in the present steel, using Ar^+ sputtering techniques (44), revealed excess thicknesses of approximately 0.01 μm at R = 0.05, which are comparable with the cyclic crack tip displacements ($\Delta CTOD$) at threshold. However, such measurements approached background noise levels and it was difficult to detect any changes in oxide thickness between the two environments or at different crack lengths.

Other models for the role of hydrogen involving hydrogen-affected plasticity (22) and hydrogen-induced Mode II crack branching (81) were discounted since no evidence of hydrogen-induced hardening or softening was seen in monotonic and cyclic tests on hydrogen-charged hour-glass specimens, nor was there any evidence of more secondary or shear cracking on fracture surface in hydrogen.

It appears, that unlike behavior in lower strength steels at low load ratios (42-44), the role of hydrogen gas, compared to moist air, in affecting near-threshold fatigue crack propagation in ultrahigh strength steels may

still be primarily associated with hydrogen embrittlement mechanisms. However, the experimental observations (Figs. 28-30) suggest that, at the partial pressures and periods (reciprocal frequency) associated with the near-threshold conditions, hydrogen uptake into the matrix, and hence the extent of embrittlement may be somewhat more efficient for water vapor compared to gaseous hydrogen. This is contrary to experience in steels at higher growth rates (27), yet similar to behavior in aluminum alloys (82), and presumably occurs because at the small ΔCTODs associated with near-threshold levels, where fretting oxidation promotes enhanced oxide growth even in nominally dry environments (44), crack tip oxide deposits may be considerably thicker than naturally-formed oxides. Since it is this nucleation and growth of oxide on the crack surface which is the source of hydrogen for water vapor environments, whereas the oxide provides a barrier for hydrogen permeation for hydrogen gas phase environments, moist air atmospheres may well be more aggressive in terms of hydrogen embrittlement mechanisms associated with near-threshold fatigue crack growth.

8. DISCUSSION AND CONCLUDING REMARKS

The present study has clearly demonstrated that the presence of corrosion products on crack faces significantly influences the fatigue behavior of lower strength steels at small stress intensity range values. At this point, it is pertinent to consider other forms of crack closure that are of importance near threshold. Since fracture morphology may be of the same size scale as the excess oxide debris on the crack faces, the possibility of crack closure arising from fracture surface roughness (55, 58) and irregular morphology (83) cannot be ignored. The work of Davidson (48) has shown that there is a strong Mode II component present at near-threshold growth rates. This implies that a rougher fracture surface would result in increased threshold ΔK values as a result of the discrete contact at several locations along the crack length (83). These different mechanisms of crack closure described above (and schematically shown in Fig. 31) (84) suggest possible explanations for the significant role near threshold of not only different environments and load ratios, but also of such other factors as yield strength (1, 4, 14) and grain size (1, 4, 59, 85) which are specific to the near-threshold regime. The role of increased strength in decreasing ΔK_o values may simply result from reduced crack closure, arising from limited plasticity-induced closure (45), less fretting (42-44) or perhaps smoother fracture surfaces (58). Certainly, higher strength steels show far less retardation in crack growth following single positive overload cycles (87), a phenomenon often explained in terms of crack closure arguments. The role of finer grain size in similarly decreasing ΔK_o values again may simply be a result of reduced crack closure from less fracture surface roughness. Such an explanation is more appealing than those based on inherent microstructural reasons where plastic zone sizes near ΔK_o are often far less than a grain diameter. Quantitative verification of these ideas is in most instances lacking, but it is interesting to note that, similar to the role of moist environments seen in the present work, the beneficial effects of lower strength and coarser microstructures in reducing near-threshold growth rates are generally far less evident, and often non-existent, at high load ratios (1, 13, 59, 84), an observation which strongly suggests a prominent role of crack closure.

No Closure   **Oxide Induced Closure**   **Roughness-Induced Closure**

K_{min}

K_{max}

K_{Cl}

$\Delta K_{eff} = K_{max} - K_{min}$ $\Delta K_{eff} = K_{max} - K_{Cl}$ $\Delta K_{eff} = K_{max} - K_{Cl}$
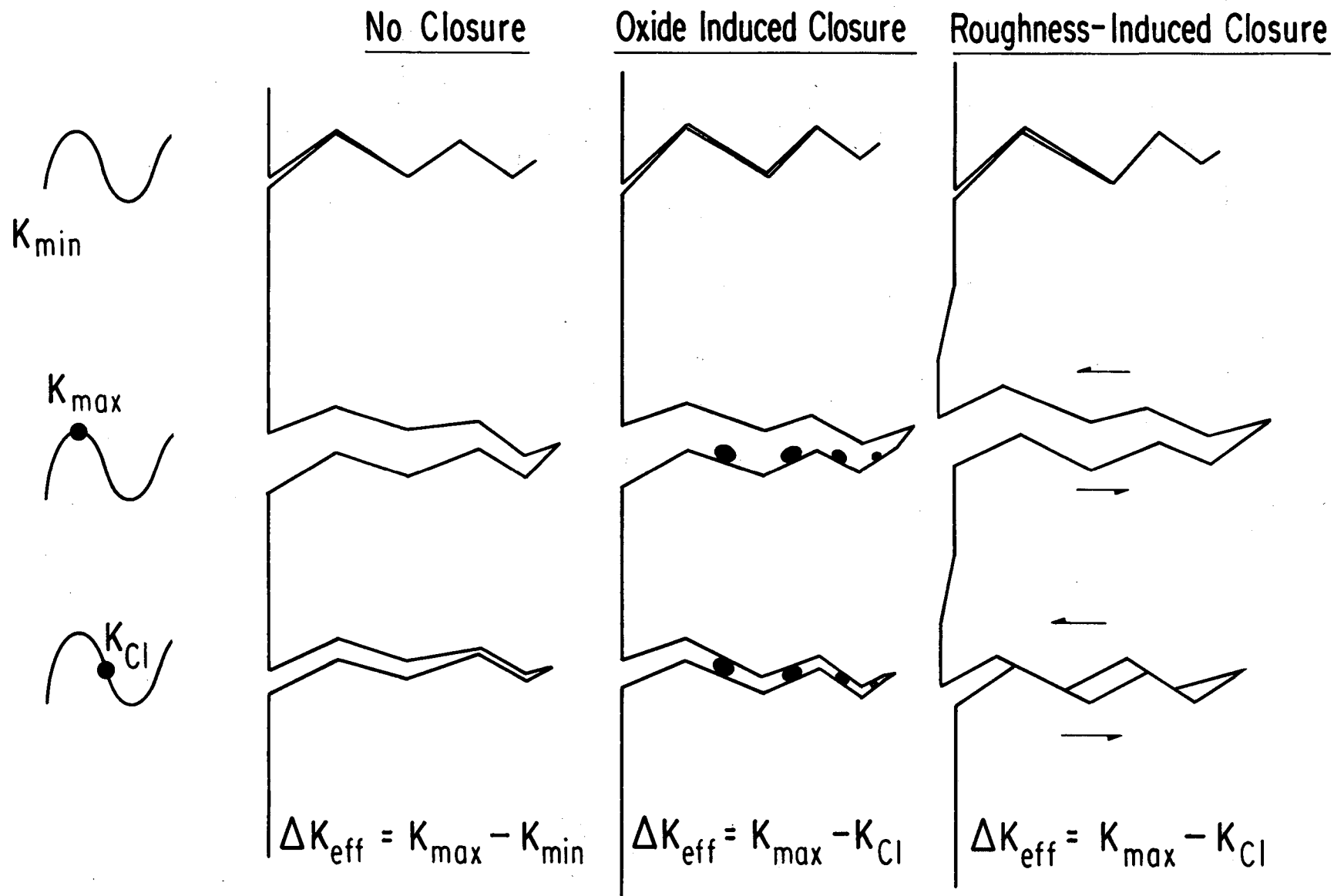
Figure 31. Schematic showing the different modes of crack closure in steels.

In summary, it is clear that concepts of crack closure are of paramount importance to fatigue crack growth behavior at near-threshold levels, although the mechanisms of such closure may be very different to the plasticity-induced closure originally proposed by Elber (45). At low stress intensities, closure mechanisms originate from the fact that pulsating crack tip opening displacements are of a size comparable with fracture surface roughness and the thickness of corrosion debris within the crack. These ideas, although still somewhat speculative at this time, suggest a very different role of alloy composition and microstructure in influencing fatigue cracking, a role which may have a profound influence on the direction which should be taken for the design of alloys with increased resistance to fatigue crack propagation at ultralow growth rates.

9. CONCLUSIONS

Based on a two-year program concerning a study of ambient temperature corrosion fatigue crack propagation in a $2\frac{1}{4}$Cr-1Mo (SA542-3) pressure vessel steel, a SA516-70 pipeline steel and an ultrahigh strength 300-M steel, the following conclusions can be made:

1. The role of gaseous hydrogen in enhancing fatigue crack propagation in lower strength steels is apparent in two distinct growth rate regimes, namely at the mid-range of growth rates (typically above $\sim 10^{-5}$ mm/cycle) and at near-threshold levels. Both regimes occur at stress intensities well below K_{Iscc}, the threshold for hydrogen-assisted cracking under sustained loads, and appear to be associated with entirely different primary mechanisms of corrosion fatigue.

2. Hydrogen-assisted crack growth in the mid-range of growth rates is characterized by an abrupt acceleration in growth rates above a critical K_{max} value, termed K_{max}^T. The acceleration is seen to be dependent upon load ratio, frequency and hydrogen pressure, and in SA542-3 is coincident with a change in fracture mode from predominately transgranular to intergranular fracture. Such enhanced crack growth rates are attributed to classical hydrogen embrittlement mechanisms, with K_{max}^T termed as the environmental threshold in fatigue for "conventional" hydrogen-assisted growth.

3. Since the value of the cyclic environmental threshold, K_{max}^T, is significantly less than K_{Iscc}, the sustained-load environmental threshold, the use of K_{Iscc} in design is considered to be highly questionable for lower strength steels.

4. The role of environment at near-threshold levels (below typically 10^{-6} mm/cycle) is seen to be markedly different in lower strength steels from conventional corrosion fatigue behavior. Although near-threshold crack growth rates are enhanced in dry hydrogen compared to moist air, the effect is only seen at low load ratios. Futhermore, growth rates are similarly enhanced in dry helium, yet somewhat decelerated in distilled water and relatively unchanged in wet hydrogen.

5. Unlikely behavior at higher, mid-range growth, there appears to be no characteristic fracture mode for environmentally-influenced crack growth at near-threshold stress intensities.

6. Near-threshold fatigue fracture surfaces are often characterized by visual corrosion deposits. Such deposits have been identified using ESCA analysis to be predominately Fe_2O_3. Using Auger spectroscopy, the thickness of the oxide deposits has been found to be inversely related to the crack growth rate, to be promoted in moist environments and at low load ratios and in general to be serveral times larger than oxide formed naturally on fresh metal surface exposed to the same environment and temperature for similar time periods.

7. Environmental influences on near-threshold growth rates in lower strength steels have been interpreted in terms of enhanced crack closure generated by such excess corrosion deposits. According to this model, termed oxide-induced crack closure, near-threshold growth rates are faster in dry environments, such as dehumidified gaseous hydrogen, primarily because of reduced crack closure effects resulting from less oxide debris formation on crack surfaces.

8. Concepts of oxide-induced closure are consistent with observed effects of load ratio, fracture morphology, and environment on near-threshold behavior in lower strength steels and further are in accordance with previous observations that inert environments accelerate near-threshold growth rates compared to distilled water, cited in the literature.

9. Despite the normal uncertainties involved in oxide thickness measurements, it can be inferred that the thickness of the excess oxide debris on the crack flanks is roughly of the order of the cyclic crack tip opening displacement at the threshold. Accordingly, one rationale for the existence of a threshold for fatigue can be considered as the stress intensity range when the crack becomes "wedged-closed" with corrosion deposits.

10. Measurement of closure near threshold using ultrasonic techniques clearly demonstrate the increased amount of closure in moist air compared to dry hydrogen, even though precise measurement of closure loads are not feasible. It is also seen that crack opening may not be a spontaneous pheonomenon, but rather gradual process with crack surfaces remaining in contact locally, while globally the crack can be considered fully open.

11. Block underload cycles at alternating stress intensities below the threshold can result in significant transient retardations in initial

growth rates when cycling is subsequently resumed at baseline ΔK_B levels, the magnitude of the effect being critically dependent upon underload (ΔK_U) and baseline (ΔK_B) stress intensitites. This behavior appears to be consistent with the arguments of oxide-induced crack closure. The lack of such crack growth retardation effects for certain combinations of underload and baseline load levels is found to occur when pulsating crack tip displacements at the underload are smaller than the existing excess oxide thicknesses.

12. In addition to mechanisms generaged by corrosion debris, sources of enhanced crack closure from fracture morphology and roughness may arise at near-threshold levels because their size-scales are comparable to crack tip displacements.

13. Studies on the ultrahigh strength 300-M alloy steel, quenched and tempered at 300°C and 650°C to tensile strengths of 2000 and 1200 MPa, respectively, reveal that, above 10^{-5} mm/cycle, the influence of hydrogen on fatigue crack gowth rates is similar to the behavior seen in lower strength SA542-3 and SA516-70 steels. While growth rates are similar in air and hydrogen at 50 Hz, the presence of hydrogen gas results in significantly faster growth rates at 5 Hz, associated with predominately intergranular cracking.

14. Below 10^{-6} mm/cycle, the presence of hydrogen gas results in slower near-threshold growth rates for the 300-M alloy, with threshold ΔK_o values 13% lower in moist air. The lower growth rates in gaseous hydrogen are observed for both tempers at 50 Hz, at high and low load ratios, and are associated with no apparent change in fracture mode.

15. Measurement of oxide deposits in ultrahigh strength steels do not indicate any enhanced build-up of corrosion debris at near-threshold levels, unlike behavior in lower strength steels.

16. The observed influence of dry gaseous hydrogen and moist air on near-threshold behavior in ultrahigh strength steels has been tentatively attributed to hydrogen embrittlement mechanisms. In the absence of any significant role of oxide-induced crack closure, hydrogen-assisted cracking in moist environments appears to be more prevalent than in gaseous hydrogen at the ultralow stress intensity ranges.

10. ACKNOWLEDGEMENTS

11. REFERENCES

1. R. O. Ritchie, _Int. Met. Reviews_, 20, 1979, p. 205.

2. H. G. Nelson, _Proc. Second Int. Cong. on Mech. Beh. Mat._, 1976, American Society for Metals, p. 690.

3. C. M. Moss, _S. M. Thesis_, M.I.T., 1979.

4. R. O. Ritchie, _Met. Sci._, 11, 1977, p.368.

5. P. C. Paris, R. J. Bucci, E. T. Wessel, W. G. Clark, and T. R. Mager, _ASTM STP 513_, 1972, p. 141.

6. R. J. Bucci, W. G. Clark, and P. C. Paris, _ibid_, p. 141.

7. R. J. Bucci, P. C. Paris, R. W. Hertzberg, R. A. Schmidt and A. F. Anderson, _ibid_, p. 125.

8. J. Mautz and V. Weiss, _ASTM STP 601_, 1976, p. 154.

9. L.K.L. Tu and B. B. Seth, _J. Test. Eval._, 6, 1978, p. 66.

10. R. J. Cooke, P. E. Irving, G. S. Booth, and C. J. Beevers, _Eng. Frac. Mech._, 7, 1975, p. 69.

11. T. C. Lindley and C. E. Richards, CEGB Note No. RD/L/N 135/78, 1978.

12. R. P. Skelton and J. R. Haigh, _Mater. Sci. Engr._, 36, 1978, p. 17.

13. R. O. Ritchie, _J. Eng. Matl. Tech._, (Trans. ASME, Series H), 99, 195 (1977).

14. G. F. Zamiski, _S. M. Thesis_, M.I.T., 1980.

15. A. Joshi, private communication, Perkin-Elmer, Surface Sciences Division, Mountain View, California, 1980.

16. M. Kurkela and R. M. Latanision, Corrosion Laboratory Report, M.I.T., 1980.

17. M. A. Devanathan and Z. Stachurski, _Proc. Roy. Soc._, 270A, 1962, p. 90.

18. R. A. Oriani and P. H. Josephic, _Acta Met._, 22, 1974, p. 1065.

19. C. Zappfe and C. Sims, _Trans. AIME_, 145, 1941, p. 225.

20. G. W. Simmons, P. S. Pao, and R. P. Wei, _Met. Trans._, 9A, 1978, p. 1147.

21. W. W. Gerberich and Y. T. Chen, _Met. Trans._, 6A, 1975, p. 271.

22. C. D. Beachem, _Met. Trans._, 3A, 1972, p.437.

23. J. P. Hirth, Met. Trans., 11A, 1980, p. 861

24. H. Cialone and R. J. Asaro, Met. Trans., 10A, 1979, p. 367.

25. R. A. Oriani and P. H. Josephic, Acta Met., 27, 1979, p. 997.

26. A. J. McEvily and R. P. Wei, in Corrosion Fatigue: Chemistry, Mechanics, and Microstructure, Proc. NACE Conf., Storrs. Conn., 1971, p. 381.

27. R. P. Wei and J. D. Landes, Mater. Res. Stds., 9, 1969, p. 25.

28. I. M. Austen and P. McIntyre, Met. Sci., 13, 1979, p. 420.

29. K. Hirano, Y. Kobayashi, H. Kobayashi, and H. Nakazawa, in Fatigue '81, Proc. SEE Conf., Warwick, Westbury House, 1981, p.87.

30. R. C. Brazill, G. W. Simmons, and R. P. Wei, J. Eng. Mat. Tech., (Trans. ASME Series H), 101, 1979, p.129.

31. M. O. Speidel, M. J. Blackburn, T. R. Beck, and J. A. Feeney, in Corrosion Fatigue: Chemistry, Mechanics, and Microstructure, Proc. NACE Conf., Storrs, Conn., 1977, p.324.

32. D. A. Meyn, Met. Trans., 2A, 1971, p. 853.

33. F. P. Ford, in Mechanical Behavior of Materials,2, Proc. 3rd Int. Conf., Cambridge, eds. K. J. Miller and R. F. Smith, Pergamon Press, 1979, p. 431.

34. D. B. Dawson and R. M. N. Pelloux, Met. Trans., 5A, 1974, p. 723.

35. B. J. Shaw and E. W. Johnson, in "Hydrogen Effects in Metals," eds. 1: M. Bernstein and A. W. Thompson, TMS-AIME, Warrendale, PA., 1981, p.691.

36. H. G. Nelson, in Effects of Hydrogen on Behavior of Materials, eds. A. W.Thompson and I. M. Bernstein, AIME, New York, 1976, p. 602.

37. H. F. Wachob and H. G. Nelson, in Hydrogen Effects in Metals. eds. I. M. Bernstein and A. W.Thompson, TMS-AIME, 1982.

38. T. R. Mager, D. M. Moon, and J. D. Landes, J. Press. Vess. Tech. (Trans. ASME Series J.), 99, 1977, p. 238.

39. W. A. Bamford and D. M. Moon, in Corrosion '79, Proc. NACE Meeting, Houston, NACE, 1979.

40. J. K. Tien, A. W. Thompson, I. M. Bernstein, and R. J. Richards, Met. Trans., 7A, 1976, p. 821.

41. F. P. Ford and T. P. Hoar, in Microstructure and Design of Alloys, 1, Proc. 3rd Int. Conf. Strength of Metals and Alloys, Cambridge, The Metals Society, 1973, p. 467.

42. R. O. Ritchie, S. Suresh, and C. M. Moss, J. Eng. Mat. Tech., (Trans. ASME Series H), 102, 1980, p. 192.

43. A. T. Stewart, Eng. Frac. Mech., 13, 1980, p. 463,

44. S. Suresh, G. F. Zamiski and R. O. Ritchie, Met. Trans., 12A, 1981, p. 1435.

45. W. Elber, ASTM STP486, 1971, p. 280.

46. S. Suresh, G. F. Zamiski, and R. O. Ritchie, ASTM STP755, 1981 (in press).

47. R. A. Schmidt and P. C. Paris, ASTM STP 536, 1973, p.79.

48. D. L. Davidson, Fat. Eng. Mat. Struct., 3, 1981, p. 229.

49. D. Benoit, R. Namdar-Tixier, and R. Tixier, Mat. Sci. Eng., 45, 1980, p.1.

50. G. L. Barenblatt, in Advances in Applied Mathematics, Academic Press, New York, VII, 1962, p. 55.

51. H. M. Westergaard, J. App. Mech. (Trans. ASME Series A), 66, 1939, p.49.

52. K. Tada, P. C. Paris, and G. R. Irwin, in Stress Analysis of Cracks Handbook, Del Research Corp., 1976.

53. S. Suresh, D. M. Parks, and R. O. Ritchie, in Fatigue Thresholds, Proc. 1st Int. Conf., Stockholm, Sweden, EMAS Publ. Ltd., Warley, 1981.

54. C. F. Shih, J. Mech. Phys. Solids, 29, 1981.

55. S. Purushothaman and J. K. Tien, in Strength of Metals and Alloys, ICSMA5 Conf. Proc., P. Haasen et.al., eds., Pergamon Press, New York, 2, 1979, p. 1267.

56. R. O. Ritchie, in Fatigue Thresholds, Proc. 1st Int. Conf., Stockholm, Sweden, EMAS Publ. Ltd., Warley, 1981.

57. C. J. Beevers, Met. Sci., 14, 1980, p. 418.

58. I. C. Mayes and T. J. Baker, in Micromechanisms of Crack Extension, The Metals Society, London, 1981.

59. G. T. Gray III, A. W. Thompson, J. C. Williams, and D. H. Stone, in Fatigue Thresholds, Proc. Int. Conf., Stockholm, Sweden, EMAS Publishers, Warley, 1981.

60. R. E. Lewis, private communication, Lockheed Palo Alto Research Labs., Palo Alto, California, 1980.

61. J. W. Swanson and H. L. Marcus, Met. Trans., 9A, 1978, p. 291

62. P. Mahulikar and H. L. Marcus, Fat. Eng. Mat. Struc., 2, 1980, p. 245.

63. G. E. Nordmark and W. G. Fricke, J. Test. Eval., 6, 1978, p. 66.

64. R. Fuquen-Molano and R. O. Ritchie, unpublished research, M.I.T., Cambridge, 1980.

65. J. H. Williams II and D. DeLonga, private communication, M.I.T., Cambridge, 1981.

66. J. D. Frandsen, R. V. Inman, and O. Buck, Int. J. Fracture, 11, 1975, p. 345.

67. V. Bachmann and D. Munz, Eng. Frac. Mech., 11, 1979, p. 61.

68. H. F. Hardrath and A. J. McEvily, Proc. Crack Prop. Symp., Cranfield, England, 1961, p.1.

69. J. Schijve and D. Broek, Aircr. Eng., 34, 1962, p. 314.

70. R. E. Jones, Eng. Frac. Mech., 5, 1973, p. 585.

71. J. R. Rice, ASTM STP 415, 1967, p. 247.

72. E. F. J. von Euw, R. W. Hertzberg, and R. Roberts, ASTM STP 513, 1972, p. 230.

73. J. Willenborg, R. M. Engle, and . A. ood, Tech. Mem. 71-1-FBR, 1971.

74. D. E. Wheeler, J. Bas. Eng., (Trans. ASME Series D), 94, 1972, p. 181.

75. R. J. Bucci, Proc. ASTM E-9/E-24 Symp. on Fatigue Crack Growth Measurement and Analysis, Pittsburgh, 1979.

76. G. A. Miller, S. J. Hudak, and R. P. Wei, J. Test Eval., 1, 1973, p.524.

77. J. F. Knott, in Fundamentals of Fracture Mechanics, Butterworths, London, 1973.

78. R. J. Bucci, Proc. 13th National Symp. Fracture Mechanics, ASTM, 1981.

79. J. Toplosky and R. O. Ritchie, Scripta Met., 15, 1981, p. 905.

80. P.K. Liaw, S. J. Hudak, and J. K. Donald, Proc. 14th National Symp. on Fracture Mechanics, UCLA, June 1981, American Society for Testing and Materials, Philadelphia.

81. Y. Takeda and C. J. McMahan, Jr., Met. Trans., 12A, 1981.

82. R. P. Wei, P. S. Pao, R. G. Hart, T. W. Weir, and G. W. Simmons, Met. Trans., 11A, 1980, p. 151.

83. N. Walker and C. J. Beevers, Fat. Eng. Mater. Struc., 1, 1979, p. 135.

84. R. O. Ritchie and S. Suresh, Met. Trans., 12A, 1981.

85. J. Masounave and J. P. Bailon, Scripta Met., 10, 1976, p. 165.

86. K. Minakawa and A. J. McEvily, Scripta Met., 15, 1981, p. 633.

87. G. J. Petrak and J. P. Gallogher, J. Eng. Matls. Tech., (Trans. ASME Ser. H) 97, 1975, p. 206.

12. PERSONNEL, PUBLICATIONS, AND THESES

The two-year research program described in this report was performed under the direction of Professor Robert O. Ritchie, principal investigator, then of the Department of Mechanical Engineering, Massachusetts Institute of Technology. The personnel involved were as follows:

i) Prof. R. O. Ritchie, principal investigator
ii) S. Suresh, research assistant (Sc. D. degree)
iii) J. Toplosky, research assistant (Sc. M. degree)
iv) T. Conley, undergraduate assistant (S. B. degree)
v) C. S. White, undergraduate assistant (S. B. degree).

A. Publications Resulting from the Work

1. *Suresh, S., Moss, C.M., and Ritchie, R. O., "Hydrogen-Assisted Fatigue Crack Growth in 2¼Cr-1Mo Low Strength Steels," Transactions of Japan Institute of Metals, 21, 481-484, 1980.

2. *Ritchie, R. O., Suresh, S., and Moss, C.M., "Near-Threshold Fatigue Crack Growth in 2¼Cr-1Mo Pressure Vessel Steel in Air and Hydrogen," Journal of Engineering Materials and Technology, Transactions of ASME Series H, 102(3), 293-299, July 1980.

3. *Suresh, S., Zamiski, G. F., and Ritchie, R. O., "Oxide-Induced Crack Closure: An Explanation for Near-Threshold Corrosion Fatigue Crack Growth Behavior," Metallurgical Transactions A, 12A (8), 1435-1443, Aug. 1981.

4. Toplosky, J., and Ritchie, R. O., "On the Influence of Gaseous Hydrogen in Decelerating Fatigue Crack Growth Rates in Ultrahigh Strength Steels," Scripta Metallurgica, 15(8), 905-908, Aug. 1981.

5. Suresh, S., and Ritchie, R.O, "Mechanisms of Environmentally-Assisted Fatigue Crack Growth in Low Strength Steels," in Advances in Fracture Research, Proceedings of Fifth International Conference on Fracture, Cannes, France, D. Francois et.al., eds., Pergamon Press, Oxford and New York, 1981, pp. 1873-1880.

6. *Ritchie, R.O., "The Application of Fracture Mechanics to Fatigue, Corrosion Fatigue and Hydrogen Embrittlement," in Analytical and Experimental Fracture Mechanics, G. C. Sih and M. Mirabile, eds., pp. 81-108, Sijthoff and Noordhoff, Holland 1981.

7. *Suresh, S., Zamiski, G. F., and Ritchie, R. O., "Fatigue Crack Propagation Behavior of 2½ Cr-1Mo Steels for Thick Wall Pressure Vessels," in <u>Application of 2¼Cr-1Mo Steel for Thick Wall Pressure Vessels</u>, ASTM STP 755, G. S. Sangdahl and M. Semchyshen, eds., American Society for Testing and Materials, Philadelphia, 1981.

8. Ritchie, R. O., and Suresh, S., "Effects of Crack Flank Oxide Debris and Fracture Surface Roughness on Near-Threshold Corrosion Fatigue," in <u>Atomistics of Fracture</u>, Proceedings of the NATO Advanced Research Institute Conference, Corsica, May 1981, R. M. Latanision, ed., Plenum Press, New York, 1981.

9. *Ritchie, R. O., "Environmental Effects on Near-Threshold Fatigue Crack Propagation in Steels: A Re-Assessment," in <u>Fatigue Thresholds</u>, Conference Proceedings, Stockholm, June 1981, J. Bäcklund, A. Blom, and C. J. Beevers, eds., EMAS Ltd., Warley, U.K. 1981.

10. Suresh, S., Parks, D. M., and Ritchie, R. O., "Crack Tip Oxide Formation and Its Influence on Fatigue Thresholds," in <u>Fatigue Thresholds</u>, Conference Proceedings, Stockholm, June 1981, J. Bäcklund, A. Blom, and C. J. Beevers, eds., EMAS Ltd., Warley, U.K. 1981.

11. Suresh, S., Toplosky, J., and Ritchie, R. O., "A Mechanism for Environmentally-Affected Near-Threshold Fatigue Crack Growth in Steels," Proceedings of 14th National Symposium on Fracture Mechanics, ASTM STP, American Society for Testing and Materials, Philadelphia, 1981.

12. Suresh, S., and Ritchie, R. O., "On the Influence of Fatigue Underloads on Cyclic Crack Growth at Low Stress Intensities," <u>Materials Science and Engineering</u>, <u>51</u>, 61-64, 1982.

13. Suresh, S., and Ritchie, R. O., "Mechanisms for the Influence of Gaseous Hydrogen on Fatigue Crack Propagation in Lower Strength Pressure Vessel and Piping Steels," <u>Acta Metallurgica</u>, submitted July 1981.

B. <u>Theses Resulting from the Work</u>

1. Suresh, S., "Mechanisms of Environmentally-Influenced Corrosion Fatigue Crack Growth in Lower Strength Steels," Sc.D. Thesis, M.I.T., 1981.

2. Toplosky, J., "Investigation into the Deceleration Due to Gaseous Hydrogen of Near-Threshold Crack Growth in an Ultrahigh Strength Steel", S.M. Thesis, M.I.T., 1981.

3. Conley, H. T., "An Accelerated K_{Iscc} Test for High-Strength Steels in Hydrogen", S.B. Thesis, M.I.T., 1980.

---

4. White, C. S., "Oxide-Induced Crack Closure of Near-Threshold Cracks," S. B. Thesis, M.I.T., 1980.

C. Other Reports

Ritchie, R.O., Suresh, S., and Toplosky, J., "Influences of Gaseous Environment on Near-Threshold Low Growth-Rate Fatigue Crack Propagation in Steels," First Annual Report to Department of Energy, Office of Basic Energy Sciences. No. DOE/ER/10389-01. (M.I.T. Fatigue and Plasticity Laboratory No. FPL/R/80/1030, Jan. 1980.)